Neuron

Article

The Temporal Association Cortex Plays a Key Role in Auditory-Driven Maternal Plasticity

Graphical Abstract

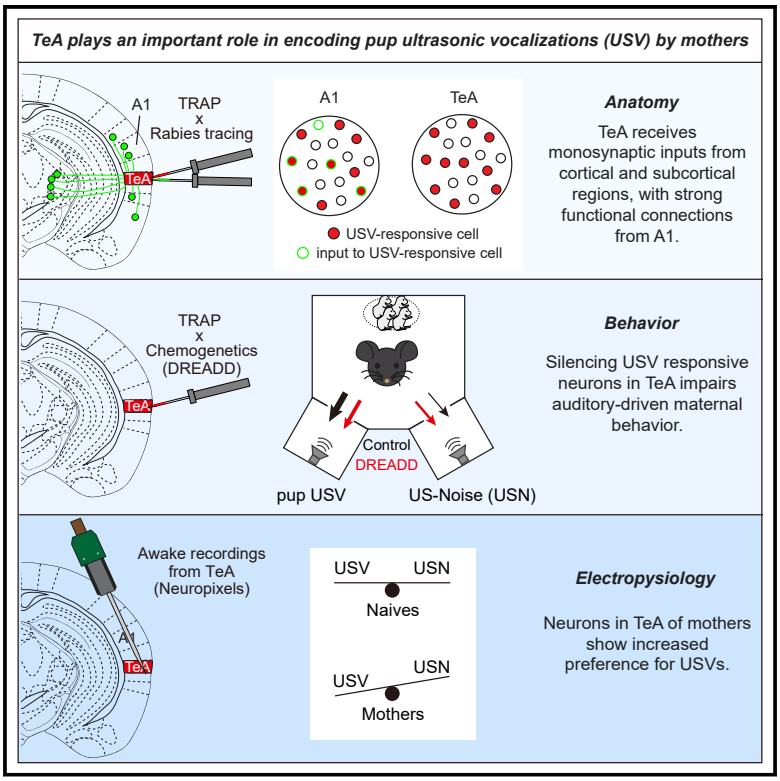

Highlights

- Temporal association cortex (TeA) is activated in response to pup calls in mothers
- TeA's connectivity is widespread, including robust functional connectivity from A1
- TeA is causally related to an auditory-driven maternal behavior by mothers
- Spiking response in TeA shows improved USV discrimination in mothers

Authors

Gen-ichi Tasaka, Libi Feigin, Ido Maor, ..., Robert C. Froemke, Liqun Luo, Adi Mizrahi

Correspondence

mizrahi.adi@mail.huji.ac.il

In Brief

Tasaka et al. show that the temporal association cortex (TeA) receives monosynaptic inputs from widespread cortical and subcortical regions. TeA shows strong functional connectivity to the primary auditory cortex. In the context of motherhood, TeA plays an important role in encoding and perceiving pup ultrasonic vocalizations by mothers.

Tasaka et al., 2020, Neuron *107*, 1–14
August 5, 2020
https://doi.org/10.1016/j.neuron.2020.05.004

CellPress

Please cite this article in press as: Tasaka et al., The Temporal Association Cortex Plays a Key Role in Auditory-Driven Maternal Plasticity, Neuron (2020), https://doi.org/10.1016/j.neuron.2020.05.004

Neuron

CellPress

Article

The Temporal Association Cortex Plays a Key Role in Auditory-Driven Maternal Plasticity

Gen-ichi Tasaka,[1] Libi Feigin,[1] Ido Maor,[1] Maya Groysman,[1] Laura A. DeNardo,[3] Jennifer K. Schiavo,[2] Robert C. Froemke,[2] Liqun Luo,[3] and Adi Mizrahi[1,4,*]

[1]Department of Neurobiology, The Edmond and Lily Safra Center for Brain Sciences, The Hebrew University of Jerusalem, Jerusalem 91904, Israel

[2]Skirball Institute for Biomolecular Medicine, Neuroscience Institute, and Department of Otolaryngology, New York University School of Medicine, New York, NY 10016, USA

[3]Department of Biology, Howard Hughes Medical Institute, Stanford University, Stanford, CA 94305, USA

[4]Lead Contact

*Correspondence: mizrahi.adi@mail.huji.ac.il

https://doi.org/10.1016/j.neuron.2020.05.004

SUMMARY

Mother-infant bonding develops rapidly following parturition and is accompanied by changes in sensory perception and behavior. Here, we study how ultrasonic vocalizations (USVs) are represented in the brain of mothers. Using a mouse line that allows temporally controlled genetic access to active neurons, we find that the temporal association cortex (TeA) in mothers exhibits robust USV responses. Rabies tracing from USV-responsive neurons reveals extensive subcortical and cortical inputs into TeA. A particularly dominant cortical source of inputs is the primary auditory cortex (A1), suggesting strong A1-to-TeA connectivity. Chemogenetic silencing of USV-responsive neurons in TeA impairs auditory-driven maternal preference in a pup-retrieval assay. Furthermore, dense extracellular recordings from awake mice reveal changes of both single-neuron and population responses to USVs in TeA, improving discriminability of pup calls in mothers compared with naive females. These data indicate that TeA plays a key role in encoding and perceiving pup cries during motherhood.

INTRODUCTION

Social interactions among animals are vital for survival and fitness of the species. Social communication cues exploit the full breadth of the senses. Visual gestures, modulation of speech, and sensitivity of touch all carry useful information during inter-animal interaction. Sensitivity to these sensory cues is critical, because they are used to interpret social context and drive specific behavioral responses. In addition, an individual's response, both its perception and its action, relies strongly on past experience and internal physiological state, which change due to past and present social interactions (Burgess et al., 2018; Carcea and Froemke, 2013). Studying the neural circuits underlying perception and how they change with experience is an entry point for understanding social engagement (Chen and Hong, 2018).

Parenting is a complex and important set of social interactions required for ensuring survival of offspring. Parenting involves physiological- and experience-dependent changes, both of which prepare the animal for better caregiving for its offspring (Dulac et al., 2014). Maternal behaviors and the neural circuits driving them have been studied for decades (Numan and Insel, 2003). Several subcortical regions and cell types therein have been causally linked to parental behaviors (Autry et al., 2019; Fang et al., 2018; Kohl et al., 2018; Wu et al., 2014). Here, we set out to study how the cortex, an important site of experience-dependent plasticity (Feldman, 2009; Rothschild and Mizrahi, 2015), processes salient sensory cues in motherhood. We focused on auditory circuits processing pup cries.

In mice, vocalizations are important cues used by pups to communicate with their parents. In particular, ultrasonic vocalizations (USVs) have been shown to convey distress and drive the mother to retrieve the vocalizing pup and return it to the nest (Ehret, 2005; Noirot, 1972). Like other sounds, pup calls are processed by the auditory system. The primary auditory cortex (A1) has been shown to undergo plasticity following motherhood (Cohen et al., 2011; Galindo-Leon et al., 2009; Liu et al., 2006; Liu and Schreiner, 2007; Marlin et al., 2015; Shepard et al., 2016; Tasaka et al., 2018). However, it is not known how maternal plasticity affects processing in higher cortical regions and to what extent other cortical regions play a role in maternal behavior. Therefore, we asked whether and how pup cries are encoded along the auditory cortical hierarchy, focusing on USVs in mothers.

To study cortical circuits involved in processing pup USVs, we combined mouse genetics, monosynaptic rabies tracing, and chemogenetic silencing of neurons during behavior. We found that a neural circuit from A1 to the temporal association cortex (TeA) is intimately involved in processing USVs and that this circuit supports maternal preference for pup calls. Using electrophysiology

Please cite this article in press as: Tasaka et al., The Temporal Association Cortex Plays a Key Role in Auditory-Driven Maternal Plasticity, Neuron (2020), https://doi.org/10.1016/j.neuron.2020.05.004

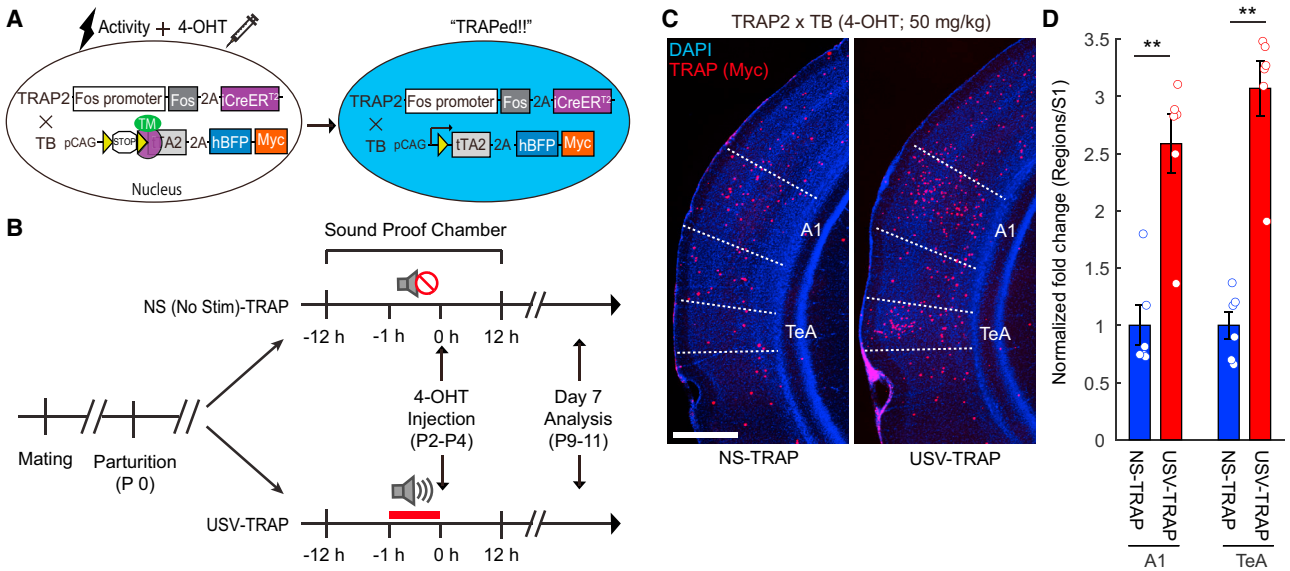

Figure 1. USVs Recruit Neurons in TeA

(A) Schematic of the TRAP × TB system.

(B) Experimental protocol used for TRAPing in mothers. Top, no stimulation (NS-TRAP). Bottom, USV stimulation (USV-TRAP).

(C) Representative fluorescent micrographs of coronal brain slices stained for TRAPed cells (Myc). Slices are from a region containing A1 and TeA, corresponding to bregma −2.92 mm in the Brain Atlas (Paxinos and Franklin, 2004). Scale bar, 500 μm.

(D) Quantification of the fold induction of TRAPed cells in A1 and TeA compared with S1 (relative density), normalized to the NS-TRAP condition (mean ± SEM; NS-TRAP, N = 6 mice; USV-TRAP, N = 6 mice; **$p < 0.01$, Mann-Whitney U test with Bonferroni correction; all statistical tests and results are listed in Table S3).

in awake mice, we measured single-neuron responses in A1 and TeA, describing how USVs are encoded in those regions. We propose that the A1-to-TeA circuit plays an important role in maternal recognition of auditory cues such as pup cries.

RESULTS

TeA Is Activated by Pup USVs

To determine which cortical regions respond to pup USVs in mothers, we used targeted recombination in active populations (TRAP), which allows permanent genetic tagging by a specific experience (Allen et al., 2017; DeNardo et al., 2019; see STAR Methods for more details). We used a previously calibrated TRAP driver system with mice expressing histone-BFP (blue fluorescent protein) as a reporter and tTA2 for additional manipulation (Figure 1A) (Tasaka et al., 2018). Playback sounds of recorded pup USVs were used to induce tagging of USV-responsive neurons, whole brains were sliced, and their cortices were analyzed for expression (Figure 1B, USV-TRAP). Control mice received no sound stimuli (no stimulation [NS]) but were otherwise identical (Figure 1B, NS-TRAP). Focusing on cortical induction, we found a 2.6 ± 0.3-fold and 3.1 ± 0.2-fold increase in A1 and TeA of mothers stimulated with USVs compared with no-sound controls, respectively (Figures 1C and 1D; NS-TRAP, N = 6 mice; USV-TRAP, N = 6 mice; values of absolute density are shown in Figure S1A). Overrepresentation of USV-TRAP cells was concentrated in the central-posterior region of A1 and TeA (Figure S1B). There were no interhemispheric differences in the number of USV-TRAP cells (Figure S1C). However, given that left asymmetry was reported in other measures by other studies (Levy et al., 2019; Marlin et al., 2015), we focused our measurements on the left hemisphere. USVs recruited TRAPed neurons in several other, putative downstream, brain regions such as the ventral and lateral orbitofrontal cortex (Figures S1D–S1F, VO and LO; Figures S1D and S1E; NS-TRAP, N = 6 mice; USV-TRAP, N = 9 mice; dataset of TRAP1 × TB [tTA2-BFP] mice). Importantly, compared with all other cortical regions tested, USV stimuli tagged relatively more neurons in TeA of mothers compared with naives (Figures S1E and S1F). In addition, we tested other pup sounds like wriggling calls (WCs), which elicit maternal responses that are distinct from USV-mediated behaviors (Ehret, 2005). Induction rate by WCs was not different between mothers and naives in all tested regions (Figure S1F). Based on these data, we hypothesized that TeA may be an important brain region for processing USVs in mothers.

The auditory TeA is located just ventral to the secondary auditory cortex and dorsal to the rhinal fissure (Paxinos and Franklin, 2004). Knowledge about the connectivity or function of TeA in any species is scarce. In contrast, A1 has been extensively studied in numerous species, including mice (Budinger and Scheich, 2009; Rothschild and Mizrahi, 2015; Theunissen and Elie, 2014). We therefore studied the anatomy and physiology of TeA with reference to the well-studied A1.

The Long-Range Presynaptic Landscape of TeA

To reveal the anatomical presynaptic input of USV-responsive neurons in TeA versus A1, we combined monosynaptic *trans*-synaptic rabies tracing with TRAP (TRAP rabies; TRAP1 and TRAP2 were used for tracing from A1 and TeA, respectively). We subcloned a new version of an optimized rabies glycoprotein oG

Please cite this article in press as: Tasaka et al., The Temporal Association Cortex Plays a Key Role in Auditory-Driven Maternal Plasticity, Neuron (2020), https://doi.org/10.1016/j.neuron.2020.05.004

(Figure 2A, AAV-CAG-FLEx-oG) (Kim et al., 2016) and used it, together with a avian sarcoma and leukemia virus receptor (TVA)-expressing virus, 3–4 weeks before TRAPing (Figure 2B; TVA^{66T} and TVA were used for tracing from A1 and TeA, respectively). We then TRAPed injected animals with USVs and, one week after TRAPing, injected pseudotyped G-deleted rabies virus into the exact site as the adeno-associated virus (AAV) injections (into either A1 or TeA; Figures 2B and 2C). We sacrificed the animals for histology five days later, verified in all mice that starter cells were predominantly restricted to the injected region (either A1 or TeA), and mapped the numbers and exact locations of GFP-expressing cells across the whole brain (Figures 2D–2H). This allowed us to visualize the presynaptic landscape onto USV-TRAP cells in A1 or TeA.

Qualitatively, the presynaptic landscape onto neurons in A1 was consistent with previous literature (Budinger and Scheich, 2009; Nelson and Mooney, 2016; Nelson et al., 2013). More specifically, inputs were detected in local circuits within the auditory cortex and in 37 distant brain locations (Table S1, USV-TRAP). Most long-range inputs to A1 were from the ventral part of the medial geniculate body (MGv) of the thalamus. Following the thalamus, most inputs came from contralateral A1, TeA, basal forebrain (BF), and neighboring cortices (Figures 2E and 2G, N = 4 mice; for the full list, see Table S1).

The input landscape of TeA was different from A1. Tracing the long-range inputs revealed ~100 brain sites sending inputs to TeA, which were both qualitatively and quantitatively distinct from the inputs into A1 (Figures 2F and 2H, N = 5 mice; for the full list, see Table S2). At a first approximation, the tracing data from TeA are consistent with traditional tracing studies showing inputs from MGv, lateral amygdala (LA), hippocampal CA1, and several sensory cortices (Arszovszki et al., 2014; Doron and Ledoux, 2000; Vaudano et al., 1991; Zingg et al., 2014). A closer analysis of our rabies-tracing data reveals new qualitative insights, as well as quantitative evaluation of the long-range input distributions. 45.3% of the inputs into TeA arise directly from A1 (Figure 2H), most of which are from layer 5 neurons (Figure S2A, red). These results suggest that TeA is, foremost, an auditory processing station directly downstream of A1. Although TeA still receives a major fraction of its inputs from the auditory cortex, its inputs are far more diverse compared with A1, particularly from subcortical regions. Monosynaptic inputs to TeA arise from various cortical and subcortical areas (the top part of the list of inputs is shown in Figure 2H). Based on this input landscape, TeA could be an integrative site of principally auditory information, with other (presumably contextual) information arriving from other cortical and subcortical brain regions.

USV-Responsive Neurons in TeA, but Not A1, Receive More Long-Range Inputs Relative to Neighboring Neurons

We next exploited TRAP-rabies to test whether the USV-responsive neurons in TeA that were TRAPed have a unique input signature. To do so, we traced USV-TRAP neurons from TeA and compared the input landscape to similar tracing from two other groups of mice: NS-TRAP and WC-TRAP. We verified that the number of starter cells and their targeting into TeA were similar among the groups (Figures 3A–3C; NS-TRAP, N = 4 mice; USV-TRAP, N = 5 mice; WC-TRAP, N = 5 mice), as was the layer distribution of starter cells in TeA (most of which were in layer 2/3 and layer 5; Figure S2B).

To quantify the long-range inputs onto TRAPed neurons, we calculated a convergence index (CI), defined as the number of input neurons in a brain region per starter cell. USV-TRAP cells had significantly higher CI values compared with NS-TRAP or WC-TRAP neurons when all input regions were considered (Figure 3D). Given that A1 is the major input region to TeA and known to respond to USVs, we hypothesized that it will be a major source of input to the USV-TRAP cells. Total inputs from A1 to USV-TRAP neurons was significantly higher compared with the NS-TRAP and WC-TRAP groups (>3-fold increase on average; Figure 3E). We assumed that the differential distribution of inputs to TeA may arise from other regions beyond A1. However, because of the larger number of brain sites that were identified and the multiple groups in the experimental design, none withstood significance after statistical correction for multiple comparisons of all regions (Figure S3A shows CI values of selected regions). To describe the relative magnitude of differences in CI between regions, we calculated d′ values from each brain region separately (using $d' = \frac{|\mu_{USV-TRAP} - \mu_{NS-TRAP}|}{\sqrt{(\sigma^2_{USV-TRAP} + \sigma^2_{NS-TRAP})/2}}$) (Figures 3F and S3B show the top part of the list that is different for USV-TRAP versus NS-TRAP inputs; for the full lists, see Table S2). Based on this analysis, we conclude that differential inputs onto USV-TRAP neurons could potentially arise from cortical and subcortical regions alike (Figure 3F). Notably, differences between USV-TRAP and WC-TRAP input landscapes were largely similar to those between USV-TRAP and NS-TRAP (compare Figure 3F, TeA, and Figure S3B). Only a few regions showed potential differences between WC-TRAP and NS-TRAP (Figure S3C). These results suggest that the USV-responsive cells receive unique functional connectivity compared with neighboring neurons.

Importantly, we conducted a similar experiment from starter cells in A1, comparing USV-TRAP to NS-TRAP mouse groups. In A1, we found no differences between the CI of USV-TRAP neurons and that of NS-TRAP neurons from any brain region (Figure 3F, A1; Figures S3D–S3H). Thus, USV-responsive neurons in TeA, but not A1, receive a particularly rich set of presynaptic inputs from long-range sources.

USV-Responsive Neurons in TeA Receive Preferential Input from USV-Responsive Neurons in A1

The combination of TRAP and rabies allows us to test functional connectivity among brain areas. We next asked whether neurons in A1 and TeA form like-to-like connections. This question would be a long-range connectivity equivalent to the well-documented like-to-like functional connectivity observed in local cortical circuits (Ko et al., 2011; Yoshimura et al., 2005). To answer this question, we analyzed TRAP-tracing data from four groups of mice: NS-TRAP, USV-TRAP, WC-TRAP, and an additional experimental group NBN-TRAP. The NBN (narrowband noise; Figure S4A) group was added as another control to USVs. Specifically, the NBN control tests connectivity among neurons responding to sounds in the spectral range of USVs but using a sound that lacks behavioral saliency.

Please cite this article in press as: Tasaka et al., The Temporal Association Cortex Plays a Key Role in Auditory-Driven Maternal Plasticity, Neuron (2020), https://doi.org/10.1016/j.neuron.2020.05.004

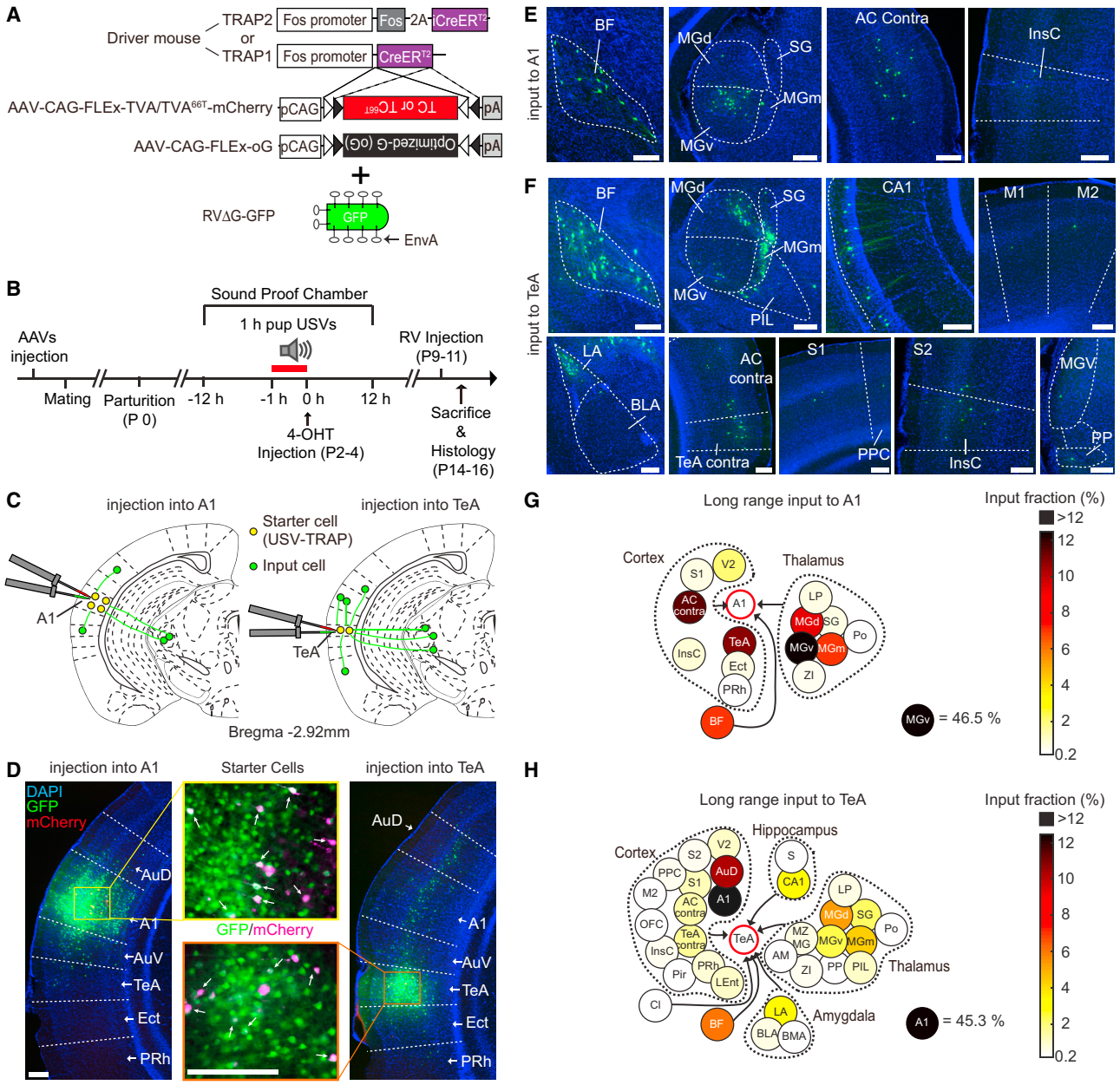

Figure 2. TeA Has a Particularly Rich Presynaptic Landscape

(A) Overview of the TRAP-rabies monosynaptic retrograde-tracing components. TRAP1 and TVA^{66T} were used for tracing from A1, and TRAP2 and TVA were used for tracing from TeA.

(B) Experimental protocol for TRAP rabies.

(C) Schematic of the TRAP-rabies experiments from two targets: A1 (left) and TeA (right). Yellow cells indicate the location of starter cells. Green cells indicate the monosynaptic inputs to the starter cells.

(D) Representative fluorescent micrographs from the injection sites in A1 (left) or TeA (right). Zoomed-in micrographs (middle) show starter cells, indicated by white arrows. Scale bar, 200 μm.

(E and F) Representative micrographs from select input regions into A1 (E) and TeA (F). Scale bar, 200 μm.

(G and H) Schematic map of selected long-range monosynaptic inputs into A1 (G) and TeA (H) (A1, N = 4 mice; TeA, N = 5 mice). Regions that received more than 0.2% of total input fraction are shown (see text and Tables S1 and S2 for full lists and abbreviations of regions). The colors indicate the proportion of each region out of the total inputs. Injection sites are shown by a red circle. The values of inputs into A1 from MGv and TeA from A1 are indicated separately, because their values exceed the color-bar scale.

Please cite this article in press as: Tasaka et al., The Temporal Association Cortex Plays a Key Role in Auditory-Driven Maternal Plasticity, Neuron (2020), https://doi.org/10.1016/j.neuron.2020.05.004

CellPress

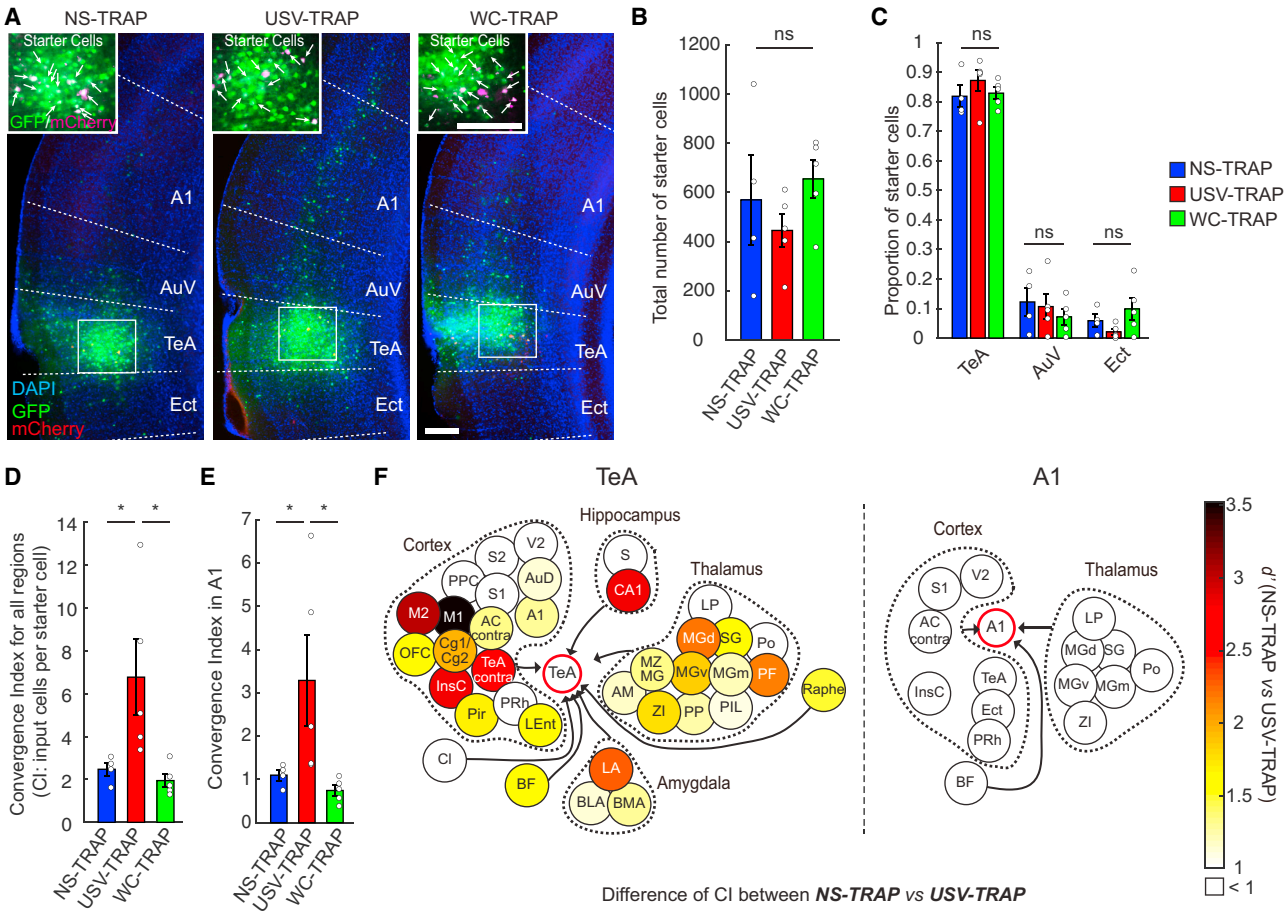

Figure 3. USV-Responsive Neurons in TeA Receive More Long-Range Inputs

(A) Representative micrographs from TeA of TRAP-rabies-injected mice. Left, NS-TRAP; middle, USV-TRAP; right, WC-TRAP. Scale bar, 200 μm.

(B and C) Total number of starter cells from NS-TRAP, USV-TRAP, and WC-TRAP mice are not different (B) (NS-TRAP, N = 4 mice; USV-TRAP, N = 5 mice; WC-TRAP, N = 5 mice; ns, not significant, Mann-Whitney U test) and spread equally in the TeA and adjacent regions (C) (ns, Mann-Whitney U test).

(D) CIs from all regions projecting into TeA for the NS-TRAP, USV-TRAP, and WC-TRAP groups. USV-TRAP had a larger CI than NS-TRAP and WC-TRAP (*$p < 0.05$, Mann-Whitney U test with Bonferroni correction).

(E) CIs from A1 into TeA for indicated groups. USV-TRAP had a larger number of inputs from A1 to TeA than NS-TRAP and WC-TRAP (*$p < 0.05$, Mann-Whitney U test with Bonferroni correction).

(F) Differential input map from TeA (left) and A1 (right) comparing USV-TRAP neurons versus the inputs of NS-TRAP neurons. Color indicates the d′ evaluated by comparing the CIs of the indicated regions for NS-TRAP and USV-TRAP animals. White regions show roughly similar CIs (d′ < 1). d′ was calculated as $d' = \frac{|\mu_{USV-TRAP} - \mu_{NS-TRAP}|}{\sqrt{\frac{\sigma^2_{USV-TRAP} + \sigma^2_{NS-TRAP}}{2}}}$. See Table S2 for abbreviations of indicated regions.

We TRAPed and traced neurons from TeA using the above-mentioned sounds and then counted how many input cells from A1 are also TRAPed. We calculated the likelihood of connection between like-to-like neurons in A1 and TeA (Figure 4; NS-TRAP, N = 4 mice; USV-TRAP, N = 5 mice; WC-TRAP, N = 5 mice; NBN-TRAP, N = 4 mice). Specifically, we measured the density of TRAP-only cells, input-only cells, and TRAP-input cells (double-labeled cells). We estimated total cell density in A1 as 109,730 cells/mm^3 (Herculano-Houzel et al., 2013; Keller et al., 2018). Using these values, we computed the probability of finding a double-labeled neuron under the assumption of independence. We used this probability to estimate the expected number of double-labeled neurons as follows:

$$\textit{Expected number of double–labeled cells} =$$

$$[\textit{Cell density in A1}] \times [\textit{Volume of ROI}] \times \Pr[\textit{TRAP cells}]$$

$$\times \Pr[\textit{Input cells}]$$

Then, we compared the observed number of double-labeled neurons with the expected number from a Poisson distribution for each group (Figure 4C, black curve, $\lambda = \textit{expected number of double–labeled cells}$). The observed number of double-labeled neurons was consistent with the assumption of independence in the NS-TRAP and NBN-TRAP groups (Figure 4C, NS-TRAP

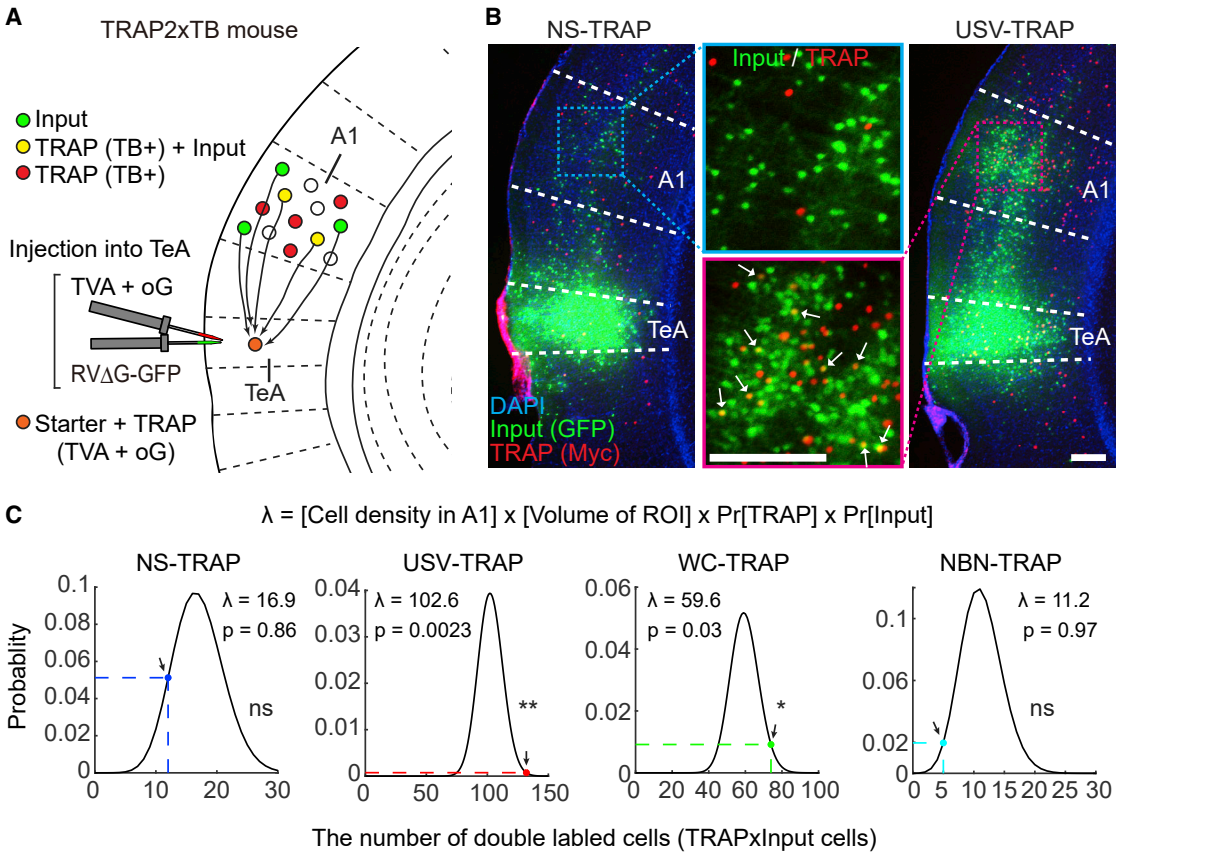

Figure 4. USV-Responsive Neurons in TeA Receive Preferential Input from USV-Responsive Neurons in A1

(A) Schematic of the analysis used to quantify the number of presynaptic cells onto TeA TRAPed neurons that are also TRAPed in A1 (yellow cells).

(B) Representative micrographs from the two TRAP-rabies experiments, injected in TeA and analyzed in A1. In A1, TRAP cells are in red (stained with anti-Myc) and green cells are presynaptic to TeA. Scale bars, 200 μm.

(C) Quantitative analysis of functional connectivity between A1 and TeA in the four experimental groups. The black curve shows the Poisson distribution estimated from the expected number of double-labeled cells as lambda. The dotted color line and an arrow indicate the observed number of double-labeled cells for each group (NS-TRAP, n = 12 cells; USV-TRAP, n = 132 cells; WC-TRAP, n = 74 cells; NBN-TRAP, n = 5 cells). USV-TRAP and WC-TRAP neurons, but not NS-TRAP and NBN-TRAP neurons, in A1 have a significantly higher probability to connect to TRAPed neurons in TeA (NS-TRAP, N = 4 mice; USV-TRAP, N = 5 mice; WC-TRAP, N = 5 mice; NBN-TRAP, N = 4 mice; *$p < 0.05$, **$p < 0.01$, extreme upper-tail probability computed by a Poisson cumulative distribution function).

[blue, p = 0.86] and NBN-TRAP [cyan, p = 0.97], extreme upper-tail probability computed by the Poisson cumulative distribution function). However, the number of double-labeled neurons was significantly larger than expected in the USV-TRAP and WC-TRAP groups (Figure 4C, USV-TRAP [red, p = 0.0023] and WC-TRAP [green, p = 0.030], extreme upper-tail probability computed by the Poisson cumulative distribution function). These results show that neurons responding to noise bursts (i.e., NBN-TRAP) or randomly TRAPed populations (i.e., NS-TRAP) are not preferentially connected but that neurons responding to natural sounds are. Thus, USV-responsive neurons in A1 are preferentially connected to USV-responsive neurons in TeA, forming a functional subnetwork from A1 to TeA.

USV-TRAP Neurons Are Causally Related to USV-Preference Behavior by Mothers

We next asked to what extent USV-responsive neurons in TeA participate in perceiving maternally salient information like pup USVs. To examine whether USV-TRAP cells in TeA are causally involved in an auditory-driven maternal behavior, we designed a behavioral paradigm based on a two-alternative forced-choice preference task of pup retrieval (Figure 5A). In short, each mother was allowed to retrieve live pups from two chambers connected to her home cage. After retrieving three pups consecutively (one from each chamber and one from the home cage), the mother was tested on a USV-preference test as follows. In one chamber, we played back USVs as the salient stimulus, and in the other chamber, we played NBN as the non-salient stimulus. Each "syllable" in the NBN encompassed a frequency band similar to that of the USVs (50–75 kHz), and the full-length stimulus had identical temporal and amplitude envelope properties (Figure S4A). Pup USVs and NBN were played simultaneously, one in each chamber, and their location changed pseudorandomly on different trials. Pups were not present in the chambers during test trials. The first chamber that the mother decided to enter was scored as her choice on

Please cite this article in press as: Tasaka et al., The Temporal Association Cortex Plays a Key Role in Auditory-Driven Maternal Plasticity, Neuron (2020), https://doi.org/10.1016/j.neuron.2020.05.004

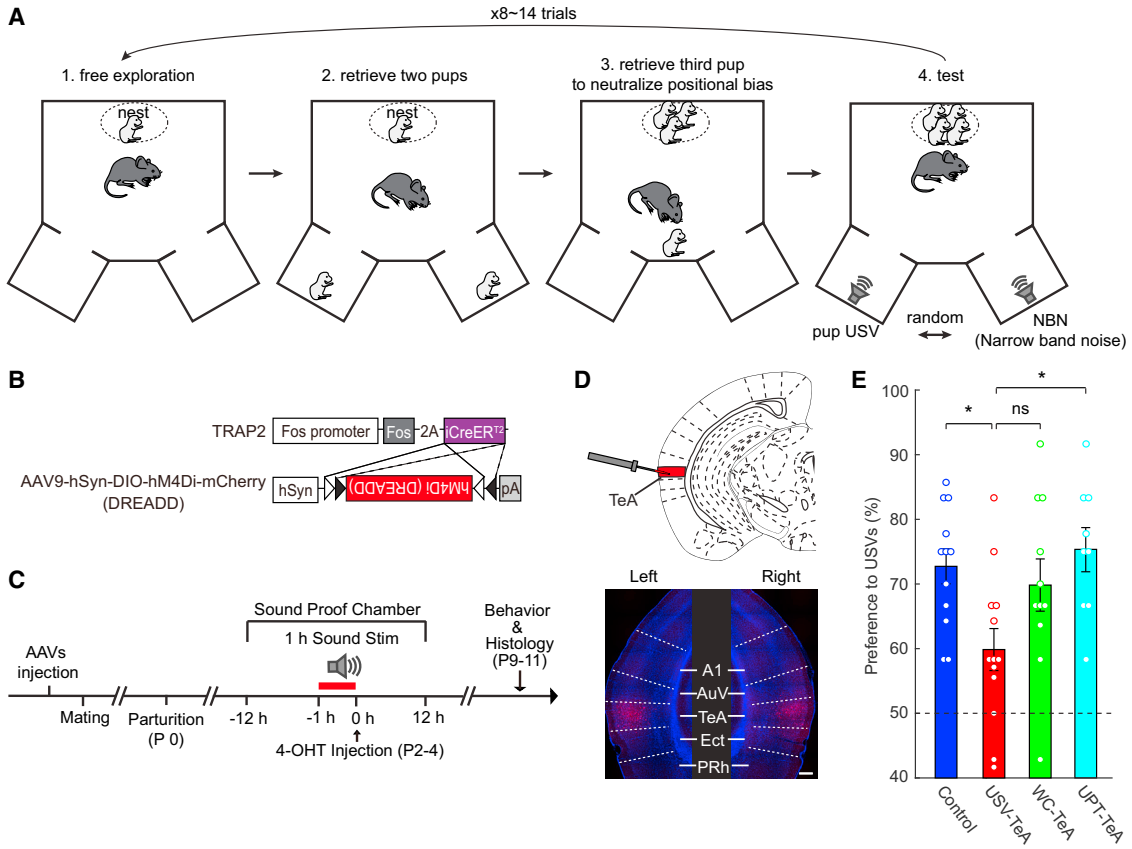

Figure 5. TeA Is Causally Related to Auditory-Driven Maternal Preference

(A) Schematic of the behavioral test.

(B) Overview of the TRAP-chemogenetic components.

(C) Experimental protocol for TRAP chemogenetics to test auditory-driven maternal behavior.

(D) Representative micrographs from DREADD-injected mice bilaterally into TeA. Left, left hemisphere; right, right hemisphere. Scale bar, 200 μm.

(E) Quantification of the maternal preference for a chamber playing USVs over NBN (mean ± SEM). Chance level is 50% (control, N = 12 mice; USV-TeA, N = 13 mice; WC-TeA, N = 11 mice; UPT-TeA, N = 9 mice; **p < 0.01; ns, not significant; Mann-Whitney U test with Bonferroni correction).

that trial. Each mother was tested on 8–14 trials (see Video S1 for one example trial).

To test whether USV-TRAP neurons in TeA had a role in this behavior, we combined TRAP and chemogenetics (TRAP-chemogenetics). We injected a Cre-dependent inhibitory designer receptor exclusively activated by designer drugs (DREADD)-encoding virus (AAV9-hSyn-DIO-hM4Di-mCherry) into TeA of TRAP mice bilaterally 3–4 weeks before TRAPing (Figures 5B–5D). Control mice were not injected with a virus before TRAPing. We injected clozapine N-oxide (CNO) into both control and experimental groups 30 min before the behavioral test. Because mothers quickly learned that pups were not present during test trials, and to compare all mothers at the same postnatal period, we compared different mice in different groups (i.e., paired analysis was not possible; Figure S4B). In a subset of mice (N = 4 mice TRAPed for USVs in A1, described later), we verified that CNO induced a decrease in the firing rates of the USV-responsive neurons (Figure S5).

Control mothers showed a preference for USVs over NBN, because they entered the chamber that was playing USVs on 72.7 ± 2.7% of the trials (Figure 5E, blue data points, N = 12 mice). Chemogenetic silencing of USV-TRAP cells in TeA decreased the maternal preference for USVs to 59.9 ± 3.2% of the trials (Figure 5E, red data points, N = 13 mice), suggesting that USV-TRAP neurons in mothers have a causal role in this task. To evaluate the extent of specificity of the USV-responsive TRAPed cells in this task, we TRAPed two additional groups of mice with different sounds. A WC-TRAP group was used as control to sounds known to induce other maternal behaviors but encompass a lower spectral range. In addition, a group of mice was TRAPed with ultrasonic pure tones (UPTs; see Figure S4A). This series of UPTs is in the spectral range of USVs but lacks the rich spectrotemporal dynamics of the syllables. We used UPTs instead of the NBN described earlier, because NBN was used as the reference stimulus in the behavioral assay.

Mice in which WC-TRAP neurons were silenced behaved similarly to the controls (Figure 5E, green data points, N = 11 mice). The WC-TRAP group was higher, but not significantly different, when compared with silencing the USV-TRAP neurons (Figure 5E, p = 0.07). This suggests that WC-TRAP neurons have a

Please cite this article in press as: Tasaka et al., The Temporal Association Cortex Plays a Key Role in Auditory-Driven Maternal Plasticity, Neuron (2020), https://doi.org/10.1016/j.neuron.2020.05.004

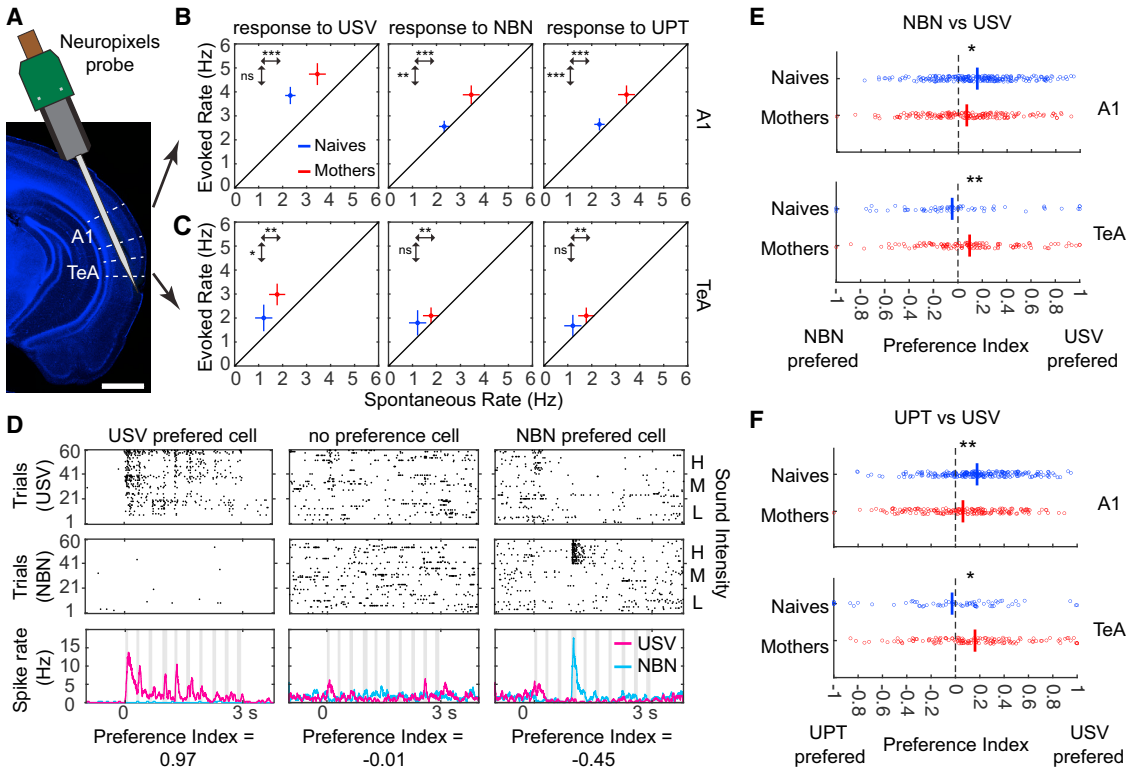

Figure 6. Distinct Plasticity of USV Coding at the Single-Cell Level in A1 and TeA

(A) Schematic of the Neuropixels probe trajectory. Scale bar, 1 mm.

(B and C) Evoked versus spontaneous spike rates of single neurons (mean ± SEM) in response to USVs, NBN, or UPTs in A1 (B) and TeA (C) (A1: naive, n = 238 cells; mother, n = 182 cells; TeA: naive, n = 69 cells; mother, n = 132 cells; *p < 0.05, **p < 0.01, ***p < 0.001; ns, not significant; Mann-Whitney U test with Bonferroni correction).

(D) Raster and PSTHs from three TeA neurons, which show different PIs (top and middle, raster plots in response to USV or NBN, respectively; bottom, PSTHs). Three sound intensities were presented 20 times for each; thus, each raster shows 60 trials. The gray bars indicate the position of syllables in the sound.

(E and F) Plots of the PIs of USVs over NBN (E) and USVs over UPTs (F) in A1 and TeA (*p < 0.05, **p < 0.01; ns, not significant; Mann-Whitney U test).

weak contribution to the USV-driven effect seen in mothers. This may be expected, because a fraction of WC-TRAP neurons are known to respond to USVs as well (Maor et al., 2016; Tasaka et al., 2018). Silencing UPT-TRAP neurons did not affect the maternal behavior (Figure 5E, cyan data points, N = 9 mice). To rule out the possibility that the behavioral effect is merely a reflection of the number of DREADD-expressing cells, we tested for correlations between the number of DREADD-expressing cells and behavioral effects. We found no such correlations across the data or in the experimental groups (Figure S6A). Finally, because viral injections are inherently leaky, we verified that most DREADD-expressing neurons were predominantly in TeA (Figures S6B and S6C). Nevertheless, we cannot rule out a small contribution of USV-TRAP neurons in other brain regions, like ventral auditory cortex (AuV) and ectorhinal cortex (Ect), to the behavioral effect (Figures S6B and S6C).

Because USV-responsive neurons in A1 are expected to drive USV neurons in TeA (Figure 4), we also TRAPed and chemogenetically silenced neurons in A1 that respond to USVs (Figures S6D–S6G). Indeed, silencing USV-TRAP neurons in A1 of mothers decreased the behavioral performance of mothers to levels similar to those of silencing USV-TRAP neurons in TeA (Figure S6E). Altogether, these results show that USV-responsive cells in TeA and A1 are causally related to maternal preference toward pup USVs.

Single-Unit Responses to USVs in A1 and TeA Following Motherhood

To this end, our experiments used TRAP and its variants as the main method suggesting that TeA is involved in encoding USVs. To assess this general conclusion using an independent and unbiased method, we next used blind electrophysiological recordings in TeA with reference to A1. We recorded spiking activity simultaneously in A1 and TeA using high-density microelectrode arrays, neuropixels probes (Figures 6A and S7A–S7D) (Jun et al., 2017). All recordings were carried out in awake, head-restrained animals. To validate the recording location, we reconstructed the trajectories of the probes after the experiments using DiI- or DiO-coated electrodes and annotated the exact regions from which we recorded in high resolution (Figures S7A–S7C) (Shamash et al., 2018). Here, we only describe responses from well-isolated single units (SUs) in response to USVs and

Please cite this article in press as: Tasaka et al., The Temporal Association Cortex Plays a Key Role in Auditory-Driven Maternal Plasticity, Neuron (2020), https://doi.org/10.1016/j.neuron.2020.05.004

for two control sounds in the same frequency range. We used both NBN and UPTs as controls, because NBN is the reference sound we played during behavior and UPTs are sounds in the same ultrasonic range.

We recorded from 5 mothers (13 probe penetrations) and 5 naive females (11 probe penetrations), for 661 SUs, out of which 40 SUs did not show response to sound and were not included in the analysis (see STAR Methods). Thus, we included 621 SUs in our dataset (naive: A1, n = 238 SU; TeA, n = 69 SU; mothers: A1, n = 182 SU; TeA, n = 132 SU). The penetration sites were similar between naives and mothers, as shown by the full reconstruction of all probes (Figure S7B). Furthermore, the distribution of the best frequencies in response to pure tones between naives and mothers was similar (Figure S7E). Response latencies to pure tones were higher in TeA, consistent with the hierarchal relationship suggested by the rabies tracing (Figure S7F). In A1, the mean spontaneous firing rates were higher in mothers as compared with naive mice, and the mean evoked responses were higher for NBN and UPTs (Figure 6B). In TeA, the mean spontaneous firing rates were higher in mothers, and the mean evoked responses were higher only in response to USVs (Figure 6C).

To test whether SUs respond preferentially to USVs versus NBN or UPTs, we calculated a preference index (PI) for each neuron as the difference between its firing rate to USVs versus either NBN or UPTs. For example, the PI of USVs versus NBN was calculated as $PI = \left(\text{firing rate}^{USV} - \text{firing rate}^{NBN}\right) / \left(\text{firing rate}^{USV} + \text{firing rate}^{NBN}\right)$. Neurons with a positive PI prefer USVs, those with a negative PI prefer NBN, and neurons with PI $\approx$ 0 respond equally to the two stimuli (see Figure 6D for three examples). In A1 of naive mice, SUs had an innate preference for USVs over NBN, which was slightly decreased in mothers (Figure 6E, top). In TeA, the transition to motherhood was accompanied by an opposite effect: on average, SUs did not prefer one stimulus over another in naives but shifted to preferring USVs over NBN in mothers (Figure 6E, bottom). Similar changes were found when comparing neuronal responses to USVs versus UPTs (Figure 6F). Thus, neurons in A1 of mothers seem to generalize similar sounds (i.e., PIs shift toward 0), and in TeA, a small yet significant discrimination develops toward USVs (i.e., PIs shift toward positive values).

Population Responses in TeA Improve USV Discrimination in Mothers

Cortical coding is likely carried out by populations of neurons. Thus, we analyzed the information from multiple simultaneously recorded neurons (Figure 7A). We first calculated pairwise peristimulus time histogram (PSTH) correlations (a measure similar to signal correlation; see STAR Methods; Maor et al., 2016), and pairwise noise correlations (NCs) (Rothschild et al., 2010). PSTH correlations describe the average similarity among neurons in responses to USVs, and pairwise NCs describe trial-to-trial variability around the mean, which has been hypothesized to reflect shared inputs (Averbeck et al., 2006). Pairwise correlations between naives and mothers differed only in TeA (Figures 7B and 7C). PSTH correlation in TeA of mothers decreased, becoming uncorrelated, compared with naives (Figure 7B; the red curve is shifted to the left and not different from shuffled data). The distribution of pairwise NCs did not differ in A1 but completely changed in TeA (Figure 7C). NCs in TeA of naives had a wide distribution, with both low and high values. After the transition to motherhood, these positive and negative correlations decreased toward zero (Figure 7C; compare the slope of the blue and red curves). Both of these results suggest that population responses in TeA become sparser; i.e., representations diverge, and trial-to-trial correlations shift toward zero.

To analyze our data beyond pairs, we calculated response vectors from all neurons that were recorded simultaneously in each mouse. Population responses from one naive female mouse and one mother are shown as three-dimensional principal-component analyses in Figure 7D, plotting responses to USV and NBN stimuli in A1 and TeA. To quantify discriminability between the sounds, we calculated Euclidean distances from the full n-dimensional space of the responses, where n is the number of neurons in each recording. The mean distance between USVs and NBN was increased in mothers, and significantly so in TeA (Figures 7E and 7F). Lastly, we evaluated the information contained in the population by calculating classification accuracy of a decoder (using a support vector machine). Decoding USVs from other stimuli in A1 was similarly high in naives and mothers (Figure 7G). Decoding USVs from the population of neurons in TeA improved in mothers when compared with both NBN and UPTs (Figure 7H). Altogether, these results show a physiological signature that favors more efficient coding of USVs compared with similar sounds in TeA of mothers.

DISCUSSION

TeA is largely an uncharted brain region. TeA is located below the somatosensory, auditory, and visual cortices and subdivided to these three sensory modalities according to its position along the rostro-caudal axis (Ramesh et al., 2018; Yamashita et al., 2018; Zingg et al., 2014). Few studies have focused on TeA in any modality. Imaging neurons in the visual TeA suggest that they form a mix of networks encoding either low-level visual features or associative outcomes like predicted value (Ramesh et al., 2018). Here, we focused on the auditory TeA (TeA for short) and studied its involvement in encoding USVs by testing natural sounds that are salient to mothers. TeA showed strong activation when mothers were exposed to USVs, as assessed by mouse genetic tools (TRAP). Combining TRAP with other methods like rabies tracing and chemogenetics showed that USV-TRAP neurons in TeA have a wide connectivity landscape and that these neurons are causally related to auditory-driven maternal behavior. Independent of TRAP, our electrophysiological recording show that neurons in TeA of mothers change in the way they encode USVs, promoting fine discrimination from similar sounds. Our work suggests that TeA plays a role in encoding pup cries during motherhood.

Functional Anatomy of TeA

The anatomy of TeA has been studied using classic anterograde and retrograde labeling, revealing that TeA receives inputs from nearly the entire neocortex and projects back to nearly the entire neocortex (Zingg et al., 2014). We found that TeA receives direct

Please cite this article in press as: Tasaka et al., The Temporal Association Cortex Plays a Key Role in Auditory-Driven Maternal Plasticity, Neuron (2020), https://doi.org/10.1016/j.neuron.2020.05.004

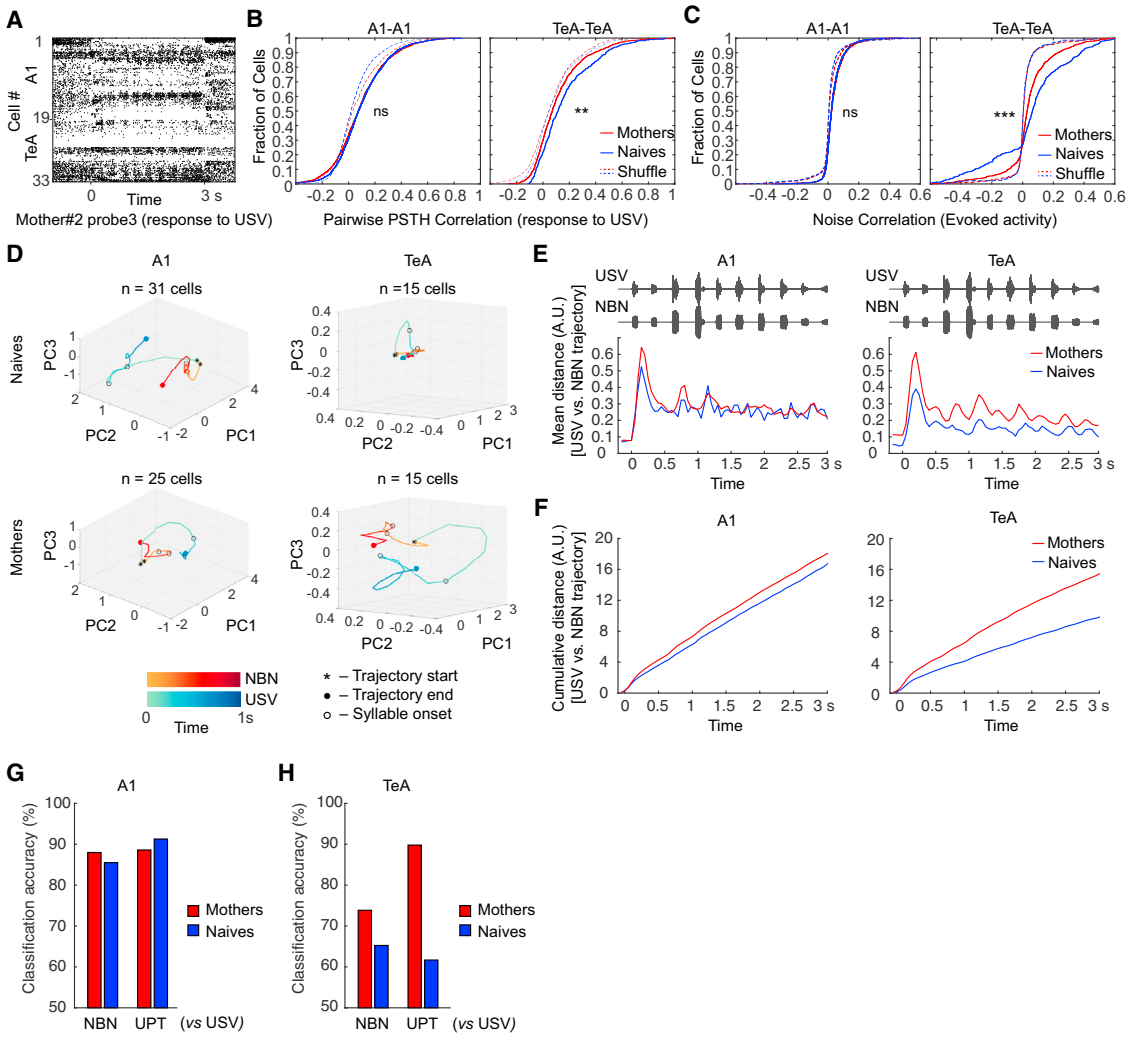

Figure 7. Distinct Plasticity of Population Coding in A1 and TeA

(A) Raster plots from one neuropixels probe recording simultaneously A1 and TeA of a mother (cells 1–19, A1; cells 20–33, TeA).

(B) Cumulative plots of pairwise PSTH correlation within regions (A1-A1: naives, n = 3,302 pairs [mean correlation = 0.10 ± 0.20]; mothers, 1,613 pairs [mean correlation = 0.09 ± 0.21]; TeA-TeA: naives, n = 409 pairs [mean correlation = 0.17 ± 0.21]; mothers, 844 pairs [mean correlation = 0.12 ± 0.19]). Dotted lines indicate shuffled PSTHs (**p < 0.01; ns, Kolmogorov-Smirnov test). All values listed here are mean ± SD.

(C) Cumulative plots of pairwise NCs (A1-A1: naives, n = 3,302 pairs [mean correlation = 0.03 ± 0.08]; mothers, 1,613 pairs [mean correlation = 0.04 ± 0.08]; TeA-TeA: naives, n = 409 pairs [mean correlation = 0.04 ± 0.33]; mothers, 844 pairs [mean correlation = 0.04 ± 0.21]). Dotted lines indicate shuffled PSTHs (***p < 0.001; ns, Kolmogorov-Smirnov test). All values listed here are mean ± SD.

(D) Trajectories of principal-component analysis (PCA) components from representative animals.

(E) Mean Euclidean distance of PCA components between USVs and NBN (red, mothers; blue, naives).

(F) Cumulative distance of PCA components between USVs and NBN.

(G) Classification performance of a support vector machine (SVM) decoder trained by the dataset of A1 neurons. The decoder was tested for its accuracy to differentiate USVs from NBN or UPTs. The decoder was trained with the first five syllables. The graphs indicate the mean value of accuracy across 1,000 iterations (USVs versus NBN: mothers, 88.0%; naives, 85.5%; USVs versus UPTs: mothers, 88.6%; naives, 91.3%).

(H) Same as (G) but in TeA (USVs versus NBN: mothers, 73.9%; naives, 65.3%; USVs versus UPTs: mothers, 89.8%; naives, 61.7%).

inputs from diverse regions across the brain and quantified these connection probabilities. Our study supports the notion that TeA is a higher-order auditory cortex, because 45% of its long-range inputs arise from A1 and it receives a high number of non-lemniscal thalamic inputs (Figures 2F–2H) (Doron and Ledoux, 2000; Lee, 2015; Romanski and LeDoux, 1993; Shi and Cassell, 1997; Vaudano et al., 1991). Yet TeA also receives a large number of non-auditory inputs from almost all other sensory cortices, as well as cognitive-related regions such as the amygdala, orbitofrontal cortex, and hippocampus (Figure 2H; Table S2). Given this diverse input landscape, it is reasonable to argue that TeA is not merely a high-order auditory cortex but rather a site that integrates sounds with other information. Because the input sources to TeA are involved in experience-dependent plasticity and

Please cite this article in press as: Tasaka et al., The Temporal Association Cortex Plays a Key Role in Auditory-Driven Maternal Plasticity, Neuron (2020), https://doi.org/10.1016/j.neuron.2020.05.004

internal or emotional states (Tye, 2018), it is well positioned to integrate auditory information with past experience, emotional state, internal state, and perhaps other sensory information, all of which are central to parenting.

TRAP tracing allowed us to reveal that neurons in TeA activated by USVs receive higher numbers of long-range inputs compared with their neighboring neurons responsive to other sounds (such as WC-TRAP) or random cells (NS-TRAP; Figure 3). The nature of these anatomical results (i.e., identification of >100 brain sites) and the relatively low number of absolute inputs from each region using rabies make it difficult to pinpoint statistical differences from specific input sources. Nevertheless, at the top of the list of putative differential inputs, we detected areas like BF, high-order auditory thalamus, LA, and hippocampus (Figures 3F and S3A, left graph). Future experiments will be needed to assess the contribution of each of these suspected pathways in isolation.

Neuromodulation is increasingly recognized as fundamental in coding of social information in the cortex, including during motherhood (Brunton and Russell, 2008; Froemke, 2015; Valtcheva and Froemke, 2019). For example, the cholinergic neurons of the BF have been shown to shape receptive field plasticity in A1 (Froemke, 2015; Froemke et al., 2007; Nelson and Mooney, 2016). Thus, how BF shapes USV responses in motherhood will be particularly interesting. Raphe nuclei too could be suspected to modulate USVs in motherhood (Figure 3F). Indeed, disruption of serotonergic neurons in raphe nuclei is known to cause impairment of maternal behaviors such as pup retrieval (Alenina et al., 2009; Lerch-Haner et al., 2008; Pawluski et al., 2019).

Other neuromodulatory systems such as dopamine, noradrenaline, and oxytocin have been reported as key drivers of parental behaviors (Fang et al., 2018; Hansen et al., 1991; Marlin et al., 2015; Numan and Smith, 1984; Thomas and Palmiter, 1997). Unfortunately, not all neuromodulatory input sources are detected by rabies tracing, because they are likely communicated by volumetric axonal release rather than by chemical synapses. For instance, we found few or no input cells onto A1 from noradrenergic neurons in the locus coeruleus or oxytocinergic neurons in the paraventricular hypothalamic nucleus, which are known to send inputs into A1 (Marlin et al., 2015; Schwarz et al., 2015). Particularly, oxytocin from the paraventricular hypothalamic nucleus has been shown to increase the response reliability to USVs in A1 of mothers by coordinating excitatory/inhibitory balance (Marlin et al., 2015). The role of neuromodulation and its impact on TeA remains an open topic to explore.

The Role of TeA in Processing Complex Sounds

TeA was initially studied in the context of acquisition and fear memory using lesions. Although the lesion studies were nonspecific to TeA, they highlighted its potential role in fear conditioning (Romanski and LeDoux, 1992). The first *in vivo* recordings from TeA were also in the context of auditory fear conditioning (Quirk et al., 1997). By comparing responses of neurons in TeA to those in the amygdala, TeA responses were found to be conditioned later and slower, suggesting that TeA encodes mnemonic or attentional information of the fear memory. Recently, work using optogenetics, supported the notion that TeA (and AuV) are not particularly critical for processing complex auditory information per se but rather causally involved in memory formation (Dalmay et al., 2019). Thus, TeA's central involvement in processing USVs could be a substrate for supporting the memory of pup cries by the parents.

Other evidence from recordings in TeA highlights its role simply as a high-order auditory cortex. Recordings from TeA in anesthetized rats (also called the suprarhinal auditory field) showed long-onset latency responses and tolerance to distortion of vocalization stimuli, implying its involvement in higher cognitive processing such as categorization (Carruthers et al., 2015; Polley et al., 2007). The sparser and decorrelated representation of USVs that we observe in TeA of mothers (Figure 7) has, at least potentially, several advantages for representing high-order information such as vocalizations (Olshausen and Field, 2004). For instance, sparse representation can be effective in pattern separation (Barlow, 1972; Olshausen and Field, 2004), or improving discrimination of complex sounds (Clemens et al., 2011), which we observed in TeA. One computation to consider is the extent of discrimination versus generalization mothers have to perform. On the one hand, mothers may benefit from generalizing to any pup call, thereby increasing their detectability regardless of the fine details they heard (Tasaka et al., 2018). On the other hand, they could benefit from the ability to better discriminate their own pup's call from those of other pups. Theoretical considerations have argued that the level of sparse coding, especially for neurons with mixed selectivity such as expected from TeA neurons, could balance the trade-off between discrimination and generalization (Barak et al., 2013). Although A1 and TeA were equally important to maternal choice toward pup calls (Figures 5 and S6), their distinct electrophysiological signatures in mothers versus naives suggest that they perform different functions. Manipulating either region alone does not necessarily tap onto the same physiological mechanism that contributes to the final choice made by the mother. Although our experiments did not reveal differences in the behavioral phenotype of silencing A1 versus silencing TeA (Figures 5 and S6), we cannot rule out that different mechanisms were perturbed in the different experiments, because the connectivities of A1 and TeA are not equal. Further experiments will be required to tease apart the relevant TeA circuits and isolate whether the A1-to-TeA connection is the central pathway contributing to this behavior.

Methodological Consideration

We used TRAP as a basis for several of our discoveries. Although TRAP has numerous advantages, it is still noisy in some aspects. TRAP has poor temporal resolution due to the multiple and often slow timescales of the molecules and reagents that drive recombination in TRAPed neurons (e.g., *c-Fos* and *4-OHT*; DeNardo and Luo, 2017). Because the TRAP signal depends on transcription, there is an inherent gap of at least several days between tagging and manipulation. Furthermore, neural networks are physiologically plastic, so not all TRAPed neurons are expected to maintain similar function when assayed days apart. New methodologies to read from and immediately manipulate neurons as the animal behaves (Carrillo-Reid et al., 2019; Jennings et al., 2019) could be instrumental in teasing out fine functional

correlations between USV-responsive neurons to maternal behavior. Nevertheless, the combination of TRAP with chemogenetics enabled the manipulation of several thousand functionally tagged neurons in a relatively homogeneous manner. Intersectional tools such as TRAP rabies or TRAP chemogenetics can be useful to elucidate the anatomy and physiology in any new brain region, as we demonstrate here for TeA.

STAR★METHODS

Detailed methods are provided in the online version of this paper and include the following:

- KEY RESOURCES TABLE
- RESOURCE AVAILABILITY
  - Lead Contact
  - Materials Availability
  - Data and Code Availability
- EXPERIMENTAL MODEL AND SUBJECT DETAILS
  - Animals
- METHOD DETAILS
  - DNA Constructs
  - Viral Procedure
  - Drug Preparation
  - Auditory Stimulation for TRAP
  - Histology
  - Counting of TRAPed cells
  - Rabies transsynaptic tracing from TRAPed cells
  - Auditory driven maternal behavior - Two-alternative forced choice task
  - Extracellular recordings using neuropixels
  - Auditory stimuli for electrophysiological recording in awake animals
  - Data Analyses - electrophysiology
  - Population data analysis
  - Decoder Analysis
  - Extracellular recordings from anesthetized animals during silencing neuronal activity
- QUANTIFICATION AND STATISTICAL ANALYSIS

SUPPLEMENTAL INFORMATION

Supplemental Information can be found online at https://doi.org/10.1016/j.neuron.2020.05.004.

ACKNOWLEDGMENTS

We thank members of the Mizrahi laboratories for comments on the manuscript and Yonatan Loewenstein and Israel Nelken for advice on statistics. We thank the Gatsby Foundation for partnering in the development of neuropixels and providing access to engineering prototype probes. We thank HHMI Janelia and UCL for helpful discussion, the development of data acquisition and analysis tools, and training in the use of Neuropixels. We gratefully acknowledge the support of the NVIDIA Corporation with the donation of the Titan Xp graphics processing unit (GPU) used for this research and the analysis of Neuropixels data. This work was supported by an ERC grant to A.M. (616063); an Israel Science Foundation (ISF) grant to A.M. (224/17); a Howard Hughes Institute Collaborative Award; a US-Israel Bi-national grant (NSF grant BRAIN EAGER) to L.L. and A.M.; and an NIH grant to L.L. (R01-NS050580). G.T. was supported by a postdoctoral fellowship from the Uehara Memorial Foundation and the Edmond and Lily Safra Center for Brain Sciences.

AUTHOR CONTRIBUTIONS

G.T. and A.M. designed experiments. L.L. and L.A.D. contributed TRAP2 mice prior to publication and provided advice. R.C.F. and J.K.S. designed the auditory-driven maternal behavior experiment. M.G. made the adeno-associated viruses. L.F. conducted the Neuropixels experiment and analyzed the data. I.M. contributed to the Neuropixels experiment. G.T. conducted all experiments and analyzed the data. G.T. and A.M. wrote the paper, with input from all authors.

DECLARATION OF INTERESTS

The authors declare no competing interests.

Received: May 6, 2019
Revised: January 29, 2020
Accepted: May 1, 2020
Published: May 29, 2020

REFERENCES

Alenina, N., Kikic, D., Todiras, M., Mosienko, V., Qadri, F., Plehm, R., Boyé, P., Vilianovitch, L., Sohr, R., Tenner, K., et al. (2009). Growth retardation and altered autonomic control in mice lacking brain serotonin. Proc. Natl. Acad. Sci. USA *106*, 10332–10337.

Allen, W.E., DeNardo, L.A., Chen, M.Z., Liu, C.D., Loh, K.M., Fenno, L.E., Ramakrishnan, C., Deisseroth, K., and Luo, L. (2017). Thirst-associated preoptic neurons encode an aversive motivational drive. Science *357*, 1149–1155.

Arszovszki, A., Borhegyi, Z., and Klausberger, T. (2014). Three axonal projection routes of individual pyramidal cells in the ventral CA1 hippocampus. Front. Neuroanat. *8*, 53.

Autry, A.E., Wu, Z., Kohl, J., Bambah-Mukku, D., Rubinstein, N.D., Marin-Rodriguez, B., Carta, I., Sedwick, V., and Dulac, C. (2019). Perifornical Area Urocortin-3 Neurons Promote Infant-directed Neglect and Aggression. bioRxiv. https://doi.org/10.1101/697334.

Averbeck, B.B., Latham, P.E., and Pouget, A. (2006). Neural correlations, population coding and computation. Nat. Rev. Neurosci. *7*, 358–366.

Barak, O., Rigotti, M., and Fusi, S. (2013). The sparseness of mixed selectivity neurons controls the generalization-discrimination trade-off. J. Neurosci. *33*, 3844–3856.

Barlow, H.B. (1972). Single units and sensation: a neuron doctrine for perceptual psychology? Perception *1*, 371–394.

Brunton, P.J., and Russell, J.A. (2008). The expectant brain: adapting for motherhood. Nat. Rev. Neurosci. *9*, 11–25.

Budinger, E., and Scheich, H. (2009). Anatomical connections suitable for the direct processing of neuronal information of different modalities via the rodent primary auditory cortex. Hear. Res. *258*, 16–27.

Burgess, C.R., Livneh, Y., Ramesh, R.N., and Andermann, M.L. (2018). Gating of visual processing by physiological need. Curr. Opin. Neurobiol. *49*, 16–23.

Carcea, I., and Froemke, R.C. (2013). Cortical Plasticity, Excitatory-Inhibitory Balance, and Sensory Perception. Prog. Brain Res. *207*, 65–90.

Carrillo-Reid, L., Han, S., Yang, W., Akrouh, A., and Yuste, R. (2019). Controlling Visually Guided Behavior by Holographic Recalling of Cortical Ensembles. Cell *178*, 447–457.e5.

Carruthers, I.M., Laplagne, D.A., Jaegle, A., Briguglio, J.J., Mwilambwe-Tshilobo, L., Natan, R.G., and Geffen, M.N. (2015). Emergence of invariant representation of vocalizations in the auditory cortex. J. Neurophysiol. *114*, 2726–2740.

Chen, P., and Hong, W. (2018). Neural Circuit Mechanisms of Social Behavior. Neuron *98*, 16–30.

Clemens, J., Kutzki, O., Ronacher, B., Schreiber, S., and Wohlgemuth, S. (2011). Efficient transformation of an auditory population code in a small sensory system. Proc. Natl. Acad. Sci. USA *108*, 13812–13817.

Cohen, L., Rothschild, G., and Mizrahi, A. (2011). Multisensory integration of natural odors and sounds in the auditory cortex. Neuron *72*, 357–369.

Dalmay, T., Abs, E., Poorthuis, R.B., Hartung, J., Pu, D.-L., Onasch, S., Lozano, Y.R., Signoret-Genest, J., Tovote, P., Gjorgjieva, J., and Letzkus, J.J. (2019). A Critical Role for Neocortical Processing of Threat Memory. Neuron *104*, 1180–1194.e7.

DeNardo, L., and Luo, L. (2017). Genetic strategies to access activated neurons. Curr. Opin. Neurobiol. *45*, 121–129.

DeNardo, L.A., Liu, C.D., Allen, W.E., Adams, E.L., Friedmann, D., Fu, L., Guenthner, C.J., Tessier-Lavigne, M., and Luo, L. (2019). Temporal evolution of cortical ensembles promoting remote memory retrieval. Nat. Neurosci. *22*, 460–469.

Doron, N.N., and Ledoux, J.E. (2000). Cells in the posterior thalamus project to both amygdala and temporal cortex: a quantitative retrograde double-labeling study in the rat. J. Comp. Neurol. *425*, 257–274.

Dulac, C., O'Connell, L.A., and Wu, Z. (2014). Neural control of maternal and paternal behaviors. Science *345*, 765–770.

Ehret, G. (2005). Infant rodent ultrasounds—a gate to the understanding of sound communication. Behav. Genet. *35*, 19–29.

Fang, Y.-Y., Yamaguchi, T., Song, S.C., Tritsch, N.X., and Lin, D. (2018). A Hypothalamic Midbrain Pathway Essential for Driving Maternal Behaviors. Neuron *98*, 192–207.e10.

Feldman, D.E. (2009). Synaptic mechanisms for plasticity in neocortex. Annu. Rev. Neurosci. *32*, 33–55.

Froemke, R.C. (2015). Plasticity of cortical excitatory-inhibitory balance. Annu. Rev. Neurosci. *38*, 195–219.

Froemke, R.C., Merzenich, M.M., and Schreiner, C.E. (2007). A synaptic memory trace for cortical receptive field plasticity. Nature *450*, 425–429.

Galindo-Leon, E.E., Lin, F.G., and Liu, R.C. (2009). Inhibitory plasticity in a lateral band improves cortical detection of natural vocalizations. Neuron *62*, 705–716.

Guenthner, C.J., Miyamichi, K., Yang, H.H., Heller, H.C., and Luo, L. (2013). Permanent genetic access to transiently active neurons via TRAP: targeted recombination in active populations. Neuron *78*, 773–784.

Hansen, S., Harthon, C., Wallin, E., Löfberg, L., and Svensson, K. (1991). Mesotelencephalic dopamine system and reproductive behavior in the female rat: effects of ventral tegmental 6-hydroxydopamine lesions on maternal and sexual responsiveness. Behav. Neurosci. *105*, 588–598.

Herculano-Houzel, S., Watson, C., and Paxinos, G. (2013). Distribution of neurons in functional areas of the mouse cerebral cortex reveals quantitatively different cortical zones. Front. Neuroanat. *7*, 35.

Jennings, J.H., Kim, C.K., Marshel, J.H., Raffiee, M., Ye, L., Quirin, S., Pak, S., Ramakrishnan, C., and Deisseroth, K. (2019). Interacting neural ensembles in orbitofrontal cortex for social and feeding behaviour. Nature *565*, 645–649.

Jun, J.J., Steinmetz, N.A., Siegle, J.H., Denman, D.J., Bauza, M., Barbarits, B., Lee, A.K., Anastassiou, C.A., Andrei, A., Aydın, Ç., et al. (2017). Fully integrated silicon probes for high-density recording of neural activity. Nature *551*, 232–236.

Keller, D., Erö, C., and Markram, H. (2018). Cell Densities in the Mouse Brain: A Systematic Review. Front. Neuroanat. *12*, 83.

Kim, E.J., Jacobs, M.W., Ito-Cole, T., and Callaway, E.M. (2016). Improved Monosynaptic Neural Circuit Tracing Using Engineered Rabies Virus Glycoproteins. Cell Rep. *15*, 692–699.

Ko, H., Hofer, S.B., Pichler, B., Buchanan, K.A., Sjöström, P.J., and Mrsic-Flogel, T.D. (2011). Functional specificity of local synaptic connections in neocortical networks. Nature *473*, 87–91.

Kohl, J., Babayan, B.M., Rubinstein, N.D., Autry, A.E., Marin-Rodriguez, B., Kapoor, V., Miyamishi, K., Zweifel, L.S., Luo, L., Uchida, N., and Dulac, C. (2018). Functional circuit architecture underlying parental behaviour. Nature *556*, 326–331.

Lee, C.C. (2015). Exploring functions for the non-lemniscal auditory thalamus. Front. Neural Circuits *9*, 69.

Lerch-Haner, J.K., Frierson, D., Crawford, L.K., Beck, S.G., and Deneris, E.S. (2008). Serotonergic transcriptional programming determines maternal behavior and offspring survival. Nat. Neurosci. *11*, 1001–1003.

Levy, R.B., Marquarding, T., Reid, A.P., Pun, C.M., Renier, N., and Oviedo, H.V. (2019). Circuit asymmetries underlie functional lateralization in the mouse auditory cortex. Nat. Commun. *10*, 2783.

Liu, R.C., and Schreiner, C.E. (2007). Auditory cortical detection and discrimination correlates with communicative significance. PLoS Biol. *5*, e173.

Liu, R.C., Linden, J.F., and Schreiner, C.E. (2006). Improved cortical entrainment to infant communication calls in mothers compared with virgin mice. Eur. J. Neurosci. *23*, 3087–3097.

Maor, I., Shalev, A., and Mizrahi, A. (2016). Distinct Spatiotemporal Response Properties of Excitatory Versus Inhibitory Neurons in the Mouse Auditory Cortex. Cereb. Cortex *26*, 4242–4252.

Maor, I., Shwartz-Ziv, R., Feigin, L., Elyada, Y., Sompolinsky, H., and Mizrahi, A. (2020). Neural Correlates of Learning Pure Tones or Natural Sounds in the Auditory Cortex. Front. Neural Circuits *13*, 82.

Marlin, B.J., Mitre, M., D'amour, J.A., Chao, M.V., and Froemke, R.C. (2015). Oxytocin enables maternal behaviour by balancing cortical inhibition. Nature *520*, 499–504.

Miyamichi, K., Shlomai-Fuchs, Y., Shu, M., Weissbourd, B.C., Luo, L., and Mizrahi, A. (2013). Dissecting local circuits: parvalbumin interneurons underlie broad feedback control of olfactory bulb output. Neuron *80*, 1232–1245.

Nelson, A., and Mooney, R. (2016). The Basal Forebrain and Motor Cortex Provide Convergent yet Distinct Movement-Related Inputs to the Auditory Cortex. Neuron *90*, 635–648.

Nelson, A., Schneider, D.M., Takatoh, J., Sakurai, K., Wang, F., and Mooney, R. (2013). A circuit for motor cortical modulation of auditory cortical activity. J. Neurosci. *33*, 14342–14353.

Noirot, E. (1972). Ultrasounds and maternal behavior in small rodents. Dev. Psychobiol. *5*, 371–387.

Numan, M., and Insel, T.R. (2003). The Neurobiology of Parental Behavior (Springer).

Numan, M., and Smith, H.G. (1984). Maternal behavior in rats: evidence for the involvement of preoptic projections to the ventral tegmental area. Behav. Neurosci. *98*, 712–727.

Olshausen, B.A., and Field, D.J. (2004). Sparse coding of sensory inputs. Curr. Opin. Neurobiol. *14*, 481–487.

Osakada, F., and Callaway, E.M. (2013). Design and generation of recombinant rabies virus vectors. Nat. Protoc. *8*, 1583–1601.

Pawluski, J.L., Li, M., and Lonstein, J.S. (2019). Serotonin and motherhood: From molecules to mood. Front. Neuroendocrinol. *53*, 100742.

Paxinos, G., and Franklin, K.B.J. (2004). The Mouse Brain in Stereotaxic Coordinates (Gulf Professional Publishing).

Polley, D.B., Read, H.L., Storace, D.A., and Merzenich, M.M. (2007). Multiparametric auditory receptive field organization across five cortical fields in the albino rat. J. Neurophysiol. *97*, 3621–3638.

Quirk, G.J., Armony, J.L., and LeDoux, J.E. (1997). Fear conditioning enhances different temporal components of tone-evoked spike trains in auditory cortex and lateral amygdala. Neuron *19*, 613–624.

Ramesh, R.N., Burgess, C.R., Sugden, A.U., Gyetvan, M., and Andermann, M.L. (2018). Intermingled Ensembles in Visual Association Cortex Encode Stimulus Identity or Predicted Outcome. Neuron *100*, 900–915.e9.

Romanski, L.M., and LeDoux, J.E. (1992). Bilateral destruction of neocortical and perirhinal projection targets of the acoustic thalamus does not disrupt auditory fear conditioning. Neurosci. Lett. *142*, 228–232.

Romanski, L.M., and LeDoux, J.E. (1993). Organization of rodent auditory cortex: anterograde transport of PHA-L from MGv to temporal neocortex. Cereb. Cortex *3*, 499–514.

Rothschild, G., and Mizrahi, A. (2015). Global order and local disorder in brain maps. Annu. Rev. Neurosci. *38*, 247–268.

Rothschild, G., Nelken, I., and Mizrahi, A. (2010). Functional organization and population dynamics in the mouse primary auditory cortex. Nat. Neurosci. *13*, 353–360.

Schwarz, L.A., Miyamichi, K., Gao, X.J., Beier, K.T., Weissbourd, B., DeLoach, K.E., Ren, J., Ibanes, S., Malenka, R.C., Kremer, E.J., and Luo, L. (2015). Viral-genetic tracing of the input-output organization of a central noradrenaline circuit. Nature *524*, 88–92.

Shamash, P., Carandini, M., Harris, K., and Steinmetz, N. (2018). A tool for analyzing electrode tracks from slice histology. bioRxiv. https://doi.org/10.1101/447995.

Shepard, K.N., Chong, K.K., and Liu, R.C. (2016). Contrast Enhancement without Transient Map Expansion for Species-Specific Vocalizations in Core Auditory Cortex during Learning. eNeuro *3*, ENEURO.0318-16.2016.

Shi, C.J., and Cassell, M.D. (1997). Cortical, thalamic, and amygdaloid projections of rat temporal cortex. J. Comp. Neurol. *382*, 153–175.

Tasaka, G.I., Guenthner, C.J., Shalev, A., Gilday, O., Luo, L., and Mizrahi, A. (2018). Genetic tagging of active neurons in auditory cortex reveals maternal plasticity of coding ultrasonic vocalizations. Nat. Commun. *9*, 871.

Theunissen, F.E., and Elie, J.E. (2014). Neural processing of natural sounds. Nat. Rev. Neurosci. *15*, 355–366.

Thomas, S.A., and Palmiter, R.D. (1997). Impaired maternal behavior in mice lacking norepinephrine and epinephrine. Cell *91*, 583–592.

Tye, K.M. (2018). Neural Circuit Motifs in Valence Processing. Neuron *100*, 436–452.

Valtcheva, S., and Froemke, R.C. (2019). Neuromodulation of maternal circuits by oxytocin. Cell Tissue Res. *375*, 57–68.

Vaudano, E., Legg, C.R., and Glickstein, M. (1991). Afferent and Efferent Connections of Temporal Association Cortex in the Rat: A Horseradish Peroxidase Study. Eur. J. Neurosci. *3*, 317–330.

Vinograd, A., Tasaka, G.I., Kreines, L., Weiss, Y., and Mizrahi, A. (2019). The Pre-synaptic Landscape of Mitral/Tufted Cells of the Main Olfactory Bulb. Front. Neuroanat. *13*, 58.

Wickersham, I.R., Lyon, D.C., Barnard, R.J., Mori, T., Finke, S., Conzelmann, K.-K., Young, J.A., and Callaway, E.M. (2007). Monosynaptic restriction of transsynaptic tracing from single, genetically targeted neurons. Neuron *53*, 639–647.

Wu, Z., Autry, A.E., Bergan, J.F., Watabe-Uchida, M., and Dulac, C.G. (2014). Galanin neurons in the medial preoptic area govern parental behaviour. Nature *509*, 325–330.

Yamashita, T., Vavladeli, A., Pala, A., Galan, K., Crochet, S., Petersen, S.S.A., and Petersen, C.C.H. (2018). Diverse Long-Range Axonal Projections of Excitatory Layer 2/3 Neurons in Mouse Barrel Cortex. Front. Neuroanat. *12*, 33.

Yoshimura, Y., Dantzker, J.L.M., and Callaway, E.M. (2005). Excitatory cortical neurons form fine-scale functional networks. Nature *433*, 868–873.

Zingg, B., Hintiryan, H., Gou, L., Song, M.Y., Bay, M., Bienkowski, M.S., Foster, N.N., Yamashita, S., Bowman, I., Toga, A.W., and Dong, H.-W. (2014). Neural networks of the mouse neocortex. Cell *156*, 1096–1111.

Please cite this article in press as: Tasaka et al., The Temporal Association Cortex Plays a Key Role in Auditory-Driven Maternal Plasticity, Neuron (2020), https://doi.org/10.1016/j.neuron.2020.05.004

CellPress

STAR★METHODS

KEY RESOURCES TABLE

REAGENT or RESOURCE	SOURCE	IDENTIFIER
Antibodies		
Mouse monoclonal anti-Myc	Santa Cruz	Cat #sc-40; RRID: AB_627268
anti-mouse donkey antibody conjugated with Cy3	Jackson ImmunoResearch	Cat #115-165-166; RRID: AB_2338692
anti-mouse donkey antibody conjugated with Alexa 647	Jackson ImmunoResearch	Cat #115-605-166; RRID: AB_2338914
Bacterial and Virus Strains		
AAV2-CAG-FLEx-TCB	ELSC vector core facility	N/A
AAV2-CAG-FLEx-TC66T	ELSC vector core facility	N/A
AAV2-CAG-FLEx-oG	ELSC vector core facility	N/A
AAV9-hSyn-DIO-hM4Di-mCherry	ELSC vector core facility	N/A
EnvA-pseudotyped, G-deleted Rabies-eGFP	This study	N/A
Chemicals, Peptides, and Recombinant Proteins		
DAPI	Santa Cruz	Cat #sc-3598
Clozapine N-oxide (CNO)	Sigma-Aldrich	Cat #C0832
Mounting Medium	Vectashield	Cat #H1000
4-OHT	Sigma-Aldrich	Cat #H6278
Corn oil	Sigma-Aldrich	Cat #C8267
DiI	Invitrogen	cat#V22885
DiO	Abcam Invitrogen	cat#ab189809 cat#V22886
Experimental Models: Cell Lines		
B7GG	Osakada and Callaway, 2013; Wickersham et al., 2007	N/A
BHK-EnvA	Osakada and Callaway, 2013; Wickersham et al., 2007	N/A
HEK293T-TVA	Osakada and Callaway, 2013; Wickersham et al., 2007	N/A
Experimental Models: Organisms/Strains		
Mouse: Fos^{CreER} (TRAP)	The Jackson Laboratory	JAX: 021882
Mouse: $Fos^{2A\text{-}iCreER}$ (TRAP2)	The Jackson Laboratory	JAX: 030323
Mouse: $Igs2^{tm5(CAG\text{-}tTA2,\text{-}TagBFP)Luo}$ (TB)	The Jackson Laboratory (Tasaka et al., 2018)	JAX: 031776
Recombinant DNA		
pAAV-CAG-FLEx-TCB	Miyamichi et al., 2013	RRID:Addgene_48331
pAAV-CAG-FLEx-TC66T	Miyamichi et al., 2013	RRID:Addgene_48332
pAAV-CAG-FLEx-oG	This study; Vinograd et al., 2019	N/A
pAAV-hSyn-DIO-hM4Di-mCherry	A gift from Bryan Roth	RRID:Addgene_50475
pAAV-EF1α-DIO-oG	A gift from Edward Callaway (Kim et al., 2016)	RRID: Addgene_74290
pAAV-CAG-FLEx-RG	Miyamichi et al., 2013	RRID: Addgene_48333
Software and Algorithms		
MATLAB	MathWorks	http://www.mathworks.com/
Photoshop	Adobe	N/A

(*Continued on next page*)

Please cite this article in press as: Tasaka et al., The Temporal Association Cortex Plays a Key Role in Auditory-Driven Maternal Plasticity, Neuron (2020), https://doi.org/10.1016/j.neuron.2020.05.004

Continued

REAGENT or RESOURCE	SOURCE	IDENTIFIER
Illustrator	Adobe	N/A
Kilosort	UCL	https://github.com/cortex-lab/KiloSort
Phy	UCL	https://github.com/kwikteam/phy-contrib
Allen Institute's Common Coordinate Framework (CCF)	Allen Institute for Brain Science	https://github.com/cortex-lab/allenCCF
Neuropixels-utils software kit	Dr. Daniel J O'shea	https://github.com/djoshea/neuropixel-utils
Other		
Nanoject 2	Drummond Scientific	Cat # 3-000-204
Programmable attenuator	TDT	PA5
Speaker driver	TDT	ED1
Speaker	TDT	EC1

RESOURCE AVAILABILITY

Lead Contact

Further information about resources, reagents used, and requests for code should be directed to and will be fulfilled by the Lead Contact, Adi Mizrahi (Mizrahi.adi@mail.huji.ac.il).

Materials Availability

This study did not generate new unique reagents.

Data and Code Availability

The datasets/code generated during this study are available from the Lead Contact upon request.

EXPERIMENTAL MODEL AND SUBJECT DETAILS

Animals

All experimental procedures were approved by the Hebrew University Animal Care and Use Committee. Mice were kept in 12-hour light-dark cycle with access to food and water *ad lib*. *TRAP1* (*Fos-CreER^{T2}* [Guenthner et al., 2013]) was obtained from the Jackson laboratories (Background strain C57BL/6). *TRAP2* (*Fos$^{2A\text{-}iCreER}$*; background strain C57BL/6) and *TB* (background strain FVB) mice were generated as detailed in earlier work (Allen et al., 2017; DeNardo et al., 2019; Tasaka et al., 2018). We used the following mouse strains: *TRAP1;TB* double heterozygous female mice (F1 hybrid of C57BL/6 and FVB strain, 8-15 weeks old) and *TRAP2;TB* double heterozygous female mice (F1 hybrid of C57BL/6 and FVB strain, 8-15 weeks old). *TRAP1;TB* mice were used for Figures S1, rabies tracing from A1 (Figures 2 and S3D–S3H), and unbiased screening of regions activated by USVs (Figures S1D–S1F; same mice that we used for Tasaka et al., 2018). We used *TRAP2;TB* mice for all other experiments.

METHOD DETAILS

DNA Constructs

pAAV-CAG-FLEx-oG was constructed as described in a previous study (Vinograd et al., 2019). Briefly, *oG* was amplified by PCR from *pAAV-EF1a-DIO-oG* (Addgene Plasmid #74290; RRID: Addgene_74290; a gift from Edward Callaway) (Kim et al., 2016) and then subcloned into *pAAV-CAG-FLEx-RG* (Addgene Plasmid #48333; RRID: Addgene_48333) (Miyamichi et al., 2013), digested with SalI and AscI. *pAAV-CAG-FLEx- TC^{66T}* and *pAAV-CAG-FLEx-TC* were gifts from Liqun Luo (Addgene Plasmid #48331 and #48332; RRID: Addgene_48331 and Addgene_48332) (Miyamichi et al., 2013). *pAAV-hSyn-DIO-hM4D(Gi)-mCherry* was a gift from Bryan Roth (Addgene plasmid #50475; http://www.addgene.org/50475/; RRID:Addgene_50475).

Viral Procedure

AAV vectors containing *CAG-FLEx-TC* (2×10^{13} genomic copies per ml), *CAG-FLEx- TC^{66T}* (2×10^{12} genomic copies per ml), *CAG-FLEx-oG* (1×10^{12} genomic copies per ml), and *hSyn-DIO-hM4D(Gi)-mCherry* (9×10^{12} genomic copies per ml) were produced by the ELSC vector core facility (EVCF). For *trans*-synaptic tracing from TRAP cells, 0.1 μL of mixture of *AAV2-CAG-FLEx-TC* or *AAV2-CAG-FLEx-TC^{66T}* and *AAV2-CAG-FLEx-oG* was stereotaxically injected into the left auditory cortex (coordinates relative to Bregma: anterior 2.5mm, lateral 4.2mm, depth 1.85mm at 20 degrees tilt from a vertical position) or into left TeA (anterior 2.7mm from Bregma,

Please cite this article in press as: Tasaka et al., The Temporal Association Cortex Plays a Key Role in Auditory-Driven Maternal Plasticity, Neuron (2020), https://doi.org/10.1016/j.neuron.2020.05.004

lateral 1.4 mm from the curvature of the bone at the boundary between the muscle and dorsal part of skull at the lateral edge) by using Nanoject 2 (Drummond Scientific). *AAV2-CAG-FLEx-TC* and *AAV2-CAG-FLEx-TC^{66T}* were used for rabies tracing from A1 and TeA, respectively. EnvA-Pseudotyped RabiesΔG (2×10^{11} infectious particles per ml) was produced following an established protocol (Osakada and Callaway, 2013; Wickersham et al., 2007). For the behavioral assay in Figures 5, 0.2 μL of *AAV9-hSyn-DIO-hM4D(Gi)-mCherry* was injected bilaterally to the auditory cortex or TeA (coordinates were the same as above for both auditory cortex and TeA).

Drug Preparation

4-hydroxytamoxifen (4-OHT; Sigma-Aldrich, Cat#H6278) was dissolved to 20 mg/mL in ethanol by shaking at 37°C for 15 min, then aliquoted and stored at −20°C for up to a month. Before use, 4-OHT was re-dissolved in ethanol by shaking at 37°C for 15 min. Corn oil (Sigma-Aldrich) was added to give a final concentration of 5 mg/mL, and the ethanol was evaporated by vacuum under centrifugation. The final 5 mg/mL 4-OHT solutions were stored at 4°C before use (for no more than 24 hours). All injections were made intraperitoneally (i.p.). 50 mg/kg 4-OHT was delivered for all TRAP experiments except for Figures S1D–S1F. In Figures S1D–S1F, 15 or 25 mg/kg 4-OHT were delivered for the experimental groups of naives or mothers, respectively.

Auditory Stimulation for TRAP

Mice were moved to a new cage more than 12 hours before injection of 4-OHT. Then the cage was placed in a sound proof-chamber (IAC Acoustics). Mothers were always cohoused with their pups during the TRAP procedure. Sound stimulation and injection of 4-OHT were conducted in a sound proof-chamber. The cage was moved back to our animal facility more than 12 hours after injection of 4-OHT. During the TRAP procedure, we rarely observed pup retrieval behaviors because the pups stayed mostly in their nest. The TRAPing sound was the dominant sound in the soundscape and the sound energy was nearly identical between the groups of naives and mothers. This suggests that any other sounds that animals produced in the cage during the TRAPing session was negligible. Additionally, TRAPing sounds did not induce any obvious observable behaviors. TRAPing is thus described as playing sounds to an awake passively-listening animal in its home cage. Sound stimuli were custom-generated in MATLAB (MathWorks) and delivered by a free field speaker (EC1, Tucker-Davis Technologies) placed above the home cage. USVs, ultrasonic pure tones (UPT), Narrow-Band-Noise (NBN) or WCs were delivered for 1 hr (total of 900 repetition of 3 s duration and ISI of 1 s). USVs (from the F2 hybrid of C57BL/6 and FVB strain) and WCs (from the C57BL/6 strain) were recorded with a one-quarter inch microphone (Brüel & Kjær) from P4–P5 pups. Additional details can be found in our previous paper (Tasaka et al., 2018). USVs contained 10 syllables. To synthesize NBN, we produced a narrow band noise at 50-75 kHz band along the time window for each syllable in the USV. The amplitude of the NBN was matched to fit the recorded USVs for each syllable. To synthesize UPT, we generated 10 log-spaced pure tones with frequencies ranging from 50 to 75 kHz. The sequence of 10 pure tones was randomized and aligned along the time window of each syllable in the USV. The amplitude was fitted to the maximum of amplitude in the USV.

Histology

Mice were given an overdose of Pental and were perfused transcardially with phosphate buffered saline (PBS) followed by 4% paraformaldehyde (PFA) in PBS. Brains were post-fixed for 12-24 hours in 4% PFA in PBS and then cryoprotected for > 24 hr in 30% sucrose in PBS. Coronal slices were made using a freezing microtome (Leica SM 2000R) and preserved in PBS. Free floating slices were then incubated in the following solutions with gentle agitation at room temperature: 2 hr in blocking solution (5% heat inactivated goat serum, 0.4% Triton X-100 in PBS); Overnight at room temperature in primary antibody 1:1000 mouse anti-Myc (Santa Cruz, Cat #sc-40, RRID: AB_627268) in blocking solution; 2-3 hr in secondary antibody 1:500 goat anti-mouse-IgG Cy3-conjugated or goat anti-mouse-IgG Alexa647-conjugated (Jackson ImmunoResearch, Cat #115-165-166 [Cy3], RRID: AB_2338692 and #115-605-166 [Alexa647], RRID: AB_2338914) in blocking solution; 15 minutes in 2.5 μg/mL of DAPI (Santa Cruz, Cat #sc-3598) in PBS. Sections were mounted on slides and coverslipped with mounting media (Vectashield H-1000). Secondary antibodies were diluted at the final concentration 1:500 from 50% glycerol stocks. Sections were imaged using an Olympus IX-81 epifluorescent microscope with a 4x and 10x objective lens (0.16 and 0.3 NA; Olympus). Images were processed in Photoshop and adjusted for contrast and brightness in each channel.

Counting of TRAPed cells

For counting the number of TRAPed cells (Figures 1 and S1A–S1C), we imaged every 50 μm 12 consecutive coronal sections through most of the rostral-caudal extent of A1 and TeA. For internal control, we imaged every 50 μm 10 consecutive coronal sections of the forelimb region of S1. Since we found no inter-hemispheric differences between left and right of A1 and TeA (Tasaka et al., 2018), we selected only the right hemisphere of A1 and TeA from each mouse for quantitative analysis. One of the left or right hemisphere of S1 was chosen for quantitative analysis for internal control. The density of TRAPed cells in both regions was calculated from the sum of the number of TRAPed cells and the volume of the regions for each slice across all sections for each animal (Figures S1A–S1C). We normalized the density of TRAPed cells in A1 and TeA to the density of TRAPed cells in S1 for each mouse. The experimental group of 'NS (No Stim) -TRAP' was set to 1 (Figure 1D).

For counting the number of TRAPed cells in downstream regions of A1 throughout the brain (Figures S1D–S1F), 40 μm coronal slices from the entire brain were immune-stained as described above. We imaged consecutively 12 coronal sections through

Please cite this article in press as: Tasaka et al., The Temporal Association Cortex Plays a Key Role in Auditory-Driven Maternal Plasticity, Neuron (2020), https://doi.org/10.1016/j.neuron.2020.05.004

most of the rostral-caudal extent of A1, TeA, and the forelimb region of S1, 6 coronal sections through prefrontal cortex including prelimbic (PrL) and orbitofrontal cortex (medial [MO], ventral [VO], lateral [LO]). We counted cells for the right A1, right TeA, left or right S1 (either right or left, chosen randomly), left and right prefrontal cortex (data from left and right were merged) for each mouse. We normalized the density of TRAPed cells in each region to the density of TRAPed cells in S1 for each mouse. The experimental group of 'NS-TRAP' was set to 1.

Rabies transsynaptic tracing from TRAPed cells

At first we injected AAVs (TC^{66T} into A1, and TC into TeA) and animals were mated several days after recovery. We then waited for animals to become lactating mothers (often more than three weeks after the AAV injection). Then, we performed TRAP at pup age P2-4. A week after TRAPing, we injected RVΔG-GFP. We sacrificed the animals 5 days after rabies injection.

For quantification of the rabies tracing data, we imaged consecutively 50 μm coronal slices along the whole brain with 4x (for long range input cells detection) and 10x (for starter cells detection) objectives. Then, we counted starter and input cells manually using a custom-written MATLAB code. We manually registered the locations and layer distribution of starter cells and input cells using a custom-written MATLAB code. The starter cells were carefully determined by their overlapped expression of TVA-mCherry and GFP. Convergence Indices were calculated by division of the number of input cells over the number of starter cells. For regional registration, boundaries were based on the Paxinos and Franklin atlas (Paxinos and Franklin, 2004). To avoid potential bias due to possible local leakage of TVA (Miyamichi et al., 2013) and given the high density of GFP labeling at the injection site, we limited our quantitative analysis to long range inputs, and excluded the two immediate neighboring cortical regions, Ect and AuV.

For counting $input^+TRAP^+$ cells, we stained consecutively 50 μm coronal slices with anti-Myc primary antibody and anti-mouse IgG Alexa-647 conjugated secondary antibody. Sections were additionally stained with DAPI. We counted the number of $input^+TRAP^-$/$input^-TRAP^+$/$input^+TRAP^+$ cells manually using a custom-written MATLAB code. To normalize across animals, we measured the volume of the counted regions in A1 of each animal. We counted all slices which contained starter cells in TeA. In Figure 4C, we calculated the expected number of $input^+TRAP^+$ cells for each group under the assumption that becoming a TRAP or an input cells are independent events as follows:

$$Expected\ number\ of\ double\text{–}labeled\ cells = [cell\ density\ in\ A1] \times [volume\ of\ ROI] \times \Pr[TRAP\ cells] \times \Pr[Input\ cells].$$

We estimated the cell density in A1 as 109,730 cells/mm^3 (Herculano-Houzel et al., 2013; Keller et al., 2018). The probability of being TRAP or input cells was calculated as the following equation:

$$\Pr[TRAP] = \frac{[observed\ number\ of\ TRAPed\ cells]}{[cell\ density\ in\ A1] \times [volume\ of\ ROI]}, \Pr[Input] = \frac{[observed\ number\ of\ input\ cells]}{[cell\ density\ in\ A1] \times [volume\ of\ ROI]}$$

We set the Poisson distribution with the sum of the expected number of double-labeled cells as lambda. Then, we calculated the complement of Poisson cumulative distribution function for the observed number of double-labeled cells in each group to estimate the upper tail probability.

Auditory driven maternal behavior - Two-alternative forced choice task

Animals were placed in a custom built Y-shape test cage (see Figure 5A; Video S1) with standard wood chip bedding. Animals had full access to food and water during the entire period. In all groups, one week after TRAPing, we habituated animals in this cage for more than 12 hours before the test. The nest was located in the center of the back wall of the main cage used for testing (Figure 5A). In an effort to maintain the original location of the nest, we transferred the nest from the old cage and placed it in the back wall of the main hall in the test cage. 120 uL of CNO (0.5 mg/mL, Sigma; C0832) was injected (i.p.) 30 min before the test. We initiated a trial by three consecutive pup retrievals. We placed one pup in the left chamber and one pup in the right chamber. After the two pups were retrieved, we placed a third pup in the center to reduce positional bias. Immediately after the retrieval of the third pup, we started to play sounds (USVs or NBN) from the speakers positioned next to the left and right chambers. USVs or NBN were played from either the left or right speaker pseudo-randomly. The stimuli were played until the animal entered one of the rooms. We determine a full body entrance into one of chambers as a choice. When animals stopped approaching the speakers, we terminated the test. Otherwise, we repeated the test for up to 14 trials.

To show that silencing USV-TRAP neurons does not affect the intact perception of ultrasonic sounds, we trained TRAPed mice to discriminate between 50 kHz and 75 kHz pure tones. Mice were TRAPed as described above using USV's (USV-TRAP) and then trained in an automated behavioral training system (see (Maor et al., 2020) for details). Following habituation, mice were trained on a go/no-go task design to lick in response to a target tone (a series of six 75 kHz pure tones, duration 100ms) in order to receive water reward and withhold licking in response to a non-target tone (a series of six 50 kHz pure tones, duration 100ms). Once mice reached a stable discrimination performance, they were injected with saline (day 11) and CNO (day 13). Their discriminability index (d') was then calculated based on the probability of licking in response to the target and non-target tones. CNO injection did not induce any significant change in discrimination, as d' values were similar between conditions and higher than the threshold for discrimination (mouse 1: d' = 1.4 and 1.4 after saline and CNO application respectively; mouse 2: d' = 1.5 and 1.2 after saline and CNO application respectively). These experiments (not shown) suggest that USV-TRAP mice are not impaired in general processing of pure tones in the ultrasound range.

Please cite this article in press as: Tasaka et al., The Temporal Association Cortex Plays a Key Role in Auditory-Driven Maternal Plasticity, Neuron (2020), https://doi.org/10.1016/j.neuron.2020.05.004

For counting the number of DREADD (hM4Di-mCherry) expressing cells in Figure S6, we imaged consecutively 40 μm slices with a 10x objective lens using an Olympus IX-81 epifluorescent microscope. We manually counted mCherry positive cells from every four sections of both hemispheres for a total of 4 or 5 slices for each using custom-written MATLAB code.

Extracellular recordings using neuropixels

For awake recording, we implanted a custom-made metal bar on the skull and performed a small craniotomy on the left hemisphere 3-4 days prior to recording day (coordinates relative to Bregma: anterior 2.5mm, lateral 4.2mm [same coordinate to the virus injections into A1]). The craniotomy was protected by the wall of dental cement and covered by silicone elastomer (WPI; Kwik-Cast cat#KWIK-CAST). After the recovery, animals were head-fixed for about 30 min to habituate to the recording setup 1-2 days before recording. On the day of the recording, animals were headfixed and the craniotomy was exposed. Then, a Neuropixels probe (imec, phase 3A) was inserted through the craniotomy and lowered down to 3 mm depth with a 20 degree tilt from a vertical position. The depth of the probes was monitored by a manipulator (Scientifica PathchStar Micromanipulator). We painted the probe with a dye (DiI [Invitrogen cat#V22885] or DiO [Invitrogen cat#V22886]), to allow us to reconstruct the penetration sites in high resolution. To annotate the brain regions according to the probe position, the exact trajectories were reconstructed from consecutive coronal slices using an open source software (Figure S7) (Shamash et al., 2018).

We acquired all recordings using Neuropixels phase 3A probes (imec), a commercially available FPGA board (KC705, Xilinx) and a base-station connector (imec). Acquisition was performed in external reference mode (Ag/AgCl wire positioned on the skull) at a sampling rate of 30 kHz, with action potential band filtered between 0.3-10 kHz. action potential band gain was set to 500. All recordings from the same animal and position were concatenated, and automatically spike sorted using the 'Kilosort' open-source software (UCL; https://github.com/cortex-lab/KiloSort). Following automatic sorting, manual sorting was performed using the 'Phy' GUI (UCL; https://github.com/kwikteam/phy-contrib). During manual sorting, spike clusters were merged based on assessment of waveform similarity and the appearance of drift patterns. Finally, each spike cluster was assessed in criteria of waveform size, waveform consistency and the presence of short-latency inter-spike-intervals (ISIs). If and only if a cluster was satisfactory on all accounts, it was tagged as a single-unit (SU) corresponding to a single neuron, and was included in the analysis. Figures S7B and S7C were generated using the software Allen CCF developed by UCL cortex-lab based on the Allen brain atlas (see https://github.com/cortex-lab/allenCCF). Figure S7D was generated using the Neuropixels-utils software kit, developed by Dan O'shea (see https://github.com/djoshea/neuropixel-utils).

Auditory stimuli for electrophysiological recording in awake animals

For recordings from awake animals, USVs, NBN, and UPT were presented 20 times at 3 attenuation levels (0, 15, 30 dB attenuation). Sound attenuation was controlled by a programmable attenuator and delivered by the speaker driver (PA5 and ED1, Tucker-Davis Technologies). The highest intensity (0 dB attenuation) was adjusted to be the same as the sound intensity of the stimuli played during TRAPing. Inter stimulus interval was set to 1 s. We also collected data in response to pure tones (3-80 kHz, 30 frequencies) and another pup calls. Our analysis here focused only on responses to USV, NBN, and UPT.

For recordings from anesthetized animals in Figure S5, USVs were presented 13-18 times at 3 attenuation levels (0, 15, 30 dB attenuation). The highest intensity (0 dB attenuation) was adjusted to be the same as the sound intensity of the stimuli played during TRAPing. Inter stimulus interval was set to 1 s. We also collected data in response to pure tones (3-80 kHz, 30 frequencies) and several pup calls. Our analysis here focused only on responses to USVs.

Data Analyses - electrophysiology

We performed all data analyses and statistics using custom-written code in MATLAB. For neuropixels recording data, we extract spiking activity using kilosort as described above. Spike times were then assigned to the local peaks of supra-threshold segments and rounded to the nearest millisecond. For each cell, we obtained a peri-stimulus time histogram (PSTH, binned at 1 ms). Evoked firing rates were extracted based on time windows of 100ms or the same size as the length of the syllable, because several syllables have a longer time window than 100ms. The values presented for evoked firing rate of each cell is the mean value of the evoked firing rate to all the syllables. The spontaneous firing rate of the cell was calculated based on the average of all 800 ms preceding each natural sounds stimulus presentation (corresponding to −1 to −0.2 s in the PSTH plots in the figures). We determined significant response to each syllable by a Mann-Whitney U test of the firing rates based on the time window of the full-width-half-maximum (FWHM) of the PSTH compared to the cell's spontaneous firing rate. The cells which had no significant response to all calls were excluded from our dataset (4, 5, 14 and 17 cells were excluded from A1-naive, A1-mother, TeA-naive and TeA-mother, respectively). Preference index in Figure 6 was calculated from the firing rate (FR) in response to two stimuli for each cell using the following equation

$$\text{Preference Index} = \frac{FR_{USV} - FR_{NBN\ or\ UPT}}{FR_{USV} + FR_{NBN\ or\ UPT}}$$

Pairwise PSTH correlations in Figure 7B were calculated as Pearson correlations between PSTHs matrices, whose spike count was binned at 20 ms.

We calculated trial-to-trial noise correlation between cells within same animals recorded simultaneously (Figure 7C). We took a 200 ms time window following the syllables' onset for calculating the single-trial responses of a neuron. Vectors containing the number of spike counts were binned at 40 ms and concatenated with all syllables. We subtracted the mean firing rate of the neuron to each sound stimulus from each single-trial response of a neuron, resulting in a vector of fluctuations around the mean responses to the different stimuli. We then used correlation coefficients between pairs of such vectors as estimates of the noise correlation between two neurons.

For best frequencies and latency analyses in Figures S7E and S7F, we first chose the subset of single units (SUs) showing significant onset excitatory responses. To identify onset responses, for each unit we looked at the 60 msec time window within a 150 msec interval beginning at stimulus onset in which the unit's firing rate was maximal. We compared the firing rates in different trials during the chosen time window to firing rates within a 60 msec time window of maximal spontaneous firing rate (chosen from the 100 msec time window preceding each stimulus presentation). All SUs that exhibited a significant onset response (t test, $p < 0.05$) were considered for the following analyses. To extract the best frequency of each unit, we first extracted the unit's frequency response area (FRA). This was done by calculating the firing rate in response to each pair of stimuli ($frequency \times attenuation$) during the unit's evoked time window, and subtracting from it the spontaneous firing rate. The frequency which evoked the maximal mean firing rate across all attenuations was defined as the unit's best frequency.

To calculate response latencies, we looked for the first 1 msec time bin in which the unit's PSTH was 2 SDs larger than its baseline response. PSTH was calculated as the mean response across all trials (from 100 msec before stimulus onsets to 600 msec following), smoothed using a 13 msec time window. The baseline response and its SD were calculated as the mean and SD of the PSTH during the 100 msec before stimulus onset. The first time bin was of stimulus onset + 5 msec (as a baseline latency to avoid false positives immediately after stimulus onset), in which the response exceeded the baseline+2SDs was considered as the unit's latency. Units which did not exhibit a response > baseline+2SD were excluded from this analysis.

Population data analysis

In order to estimate the ability of a network to discriminate between USVs and NBN, we started by calculating pairwise Euclidean distances and d primes for each group of simultaneously recorded units. Prior to the calculation, raster plots were binned into 50 msec bins. For each group of simultaneously recorded units, the response difference vector was calculated for each time bin according to:

$$\Delta\mathrm{resp(t)} = \mu(USVresp(t)) - \mu(NBNresp(t))$$

Where μ is the mean response of the population for the given stimulus, and is a ($1 \times n$) vector, where n is the number of units in a given recording. t refers to a specific time bin. The Euclidean distance between trajectories was calculated as the norm of the difference vector divided by the square root of the number of units contributing to the distance measure (in order to normalize the distance).

$$\mathrm{dist(t)} = \frac{|\Delta\mathrm{resp(t)}|}{\sqrt{n}}$$

To calculate the mean distance for a given time bin across all the population of recorded units, we created a weighted average of the distances, scaled by the number of contributing units in each recording

$$\mu(dist, t) = \frac{\sum_{i=1}^{N} dist_i(t) \cdot n_i}{\sum_{i=1}^{N} n_i}$$

Where N is the total number of recordings, and $dist_i$ and n_i are the trajectory distance and number of units in a given recording. Cumulative distance was calculated by calculating the area under the curve up to bin t.

PCA analysis was used to demonstrate the divergence of responses to USV's and NBN. For every population of simultaneously recorded units a time series of all trials for both stimuli was constructed to give a (n x (n-$trials$ * $time$-$bins$-per-$trial$)) matrix (where n is the number of units in the population, and the number of trials is 80 as we use 40 trials from each stimulus type). The first 3 PCs were calculated for the entire time series, and their coefficients for every time bin were extracted. The mean trajectory in PCA space for each stimulus type was plotted on top of a 3D axis (Figure 7D).

Decoder Analysis

Classification of call identity using population activity was performed using a Support Vector Machine (SVM) classifier with a linear kernel. The input to a SVM consisted of the spike count of each neuron in the 100 ms or as the same length of the syllable (i.e., if the syllable has a longer duration than 100 ms) following syllable onset. Thus, a response vector to the stimulus is composed of each neuron's spike count to each of the first syllables of a stimulus up to some number of syllables. In each run, 60% of the data (12 trials from the lowest sound intensity) were used for training and 40% of the trials (8 trials from the lowest sound intensity) were used as the test set for decoding accuracy. Each classifier was iterated 1000 times and a mean accuracy was calculated. Different combinations of trials were chosen randomly for each run. We increased the number of syllables cumulatively from 1 up to 10 for each sound stimulus to measure the accuracy at an increasing number of syllables. In Figures 7G and 7H, we show the accuracy at 5 syllables

because the decoder accuracy reached plateau around 5 syllables. We ran 4 classifiers – 2 different populations (A1 and TeA), comparing a USV stimulus against NBN and UPT.

Extracellular recordings from anesthetized animals during silencing neuronal activity

We performed extracellular recordings in anesthetized animals while silencing TRAPed cells in A1 by DREADDs (Figure S5). Those animals were anesthetized with an i.p. injection of ketamine and medetomidine (80 mg/kg and 0.65 mg/kg, respectively) and a subcutaneous injection of Carprofen (0.004 mg/g). The depth of anesthesia was assessed by monitoring the pinch withdrawal reflex and ketamine/medetomidine was added to maintain it. The animal's rectal temperature was continuously monitored and maintained at 36°C ± 1°C. For recording, a custom made metal pin was glued to the skull using dental cement, and connected to a custom stage to allow precise positioning of the head relative to the speaker (facing the right ear). A small craniotomy was performed on the left hemisphere (coordinates relative to Bregma: anterior 2.5 mm, lateral 4.2 mm). Then, a neuropixels probe was inserted through this craniotomy and lowered down to a 3 mm depth with a 20 degree tilt from a vertical position. We painted the probe with a dye (DiI, [Invitrogen cat#V22885] or DiO [Abcam #ab189809]), to allow us to reconstruct the penetration sites in high resolution. To silence neural activity by DREADDs, 120 uL of CNO (0.5 mg/mL, Sigma; C0832) was injected i.p. after the first delivery of a sound protocol (pre CNO session). 30 min after the injection of CNO, the same sound protocol was delivered (post CNO session). Spike sorting and data analysis were performed in the same way as described above.

QUANTIFICATION AND STATISTICAL ANALYSIS

Statistical tests were performed using MATLAB. All tests were two-tailed. The sample size and statistical tests used are indicated in the figure legends. A full report of P values and performed statistical tests were summarized in Table S3. To correct for multiple comparisons, we used Bonferroni correction for less than five simultaneous comparisons and Benjamini-Hochberg correction for more than five simultaneous comparisons. Benjamini-Hochberg correction was based on the codes at MATLAB central file exchange (https://www.mathworks.com/matlabcentral/fileexchange/27418-fdr_bh, MATLAB Central File Exchange). Criteria for statistical significance is set at $p < 0.05$.